Importance of extracellular vimentin in the dynamics of pathogen invasion

Jannatun Irana Ira

MATH 8996 - Final Project

in partial fulfilment of the requirements of the degree of

Master of Science

Department of Mathematics

University of Manitoba

Abstract:

Vimentin is a type III intermediate filament protein that plays a crucial role in the structural integrity and function of the cell's cytoskeleton. It is involved in essential cellular processes such as maintaining cell shape, enabling cell migration, supporting cell division, promoting wound healing, and facilitating tissue development. In addition to these intracellular functions, a growing body of research highlights the significance of extracellular vimentin in various physiological and pathological contexts. In the extracellular environment, vimentin can exist in multiple forms: either as a filamentous or non-filamentous protein, attached to the cell surface, or present in a soluble exogenous state. One particularly intriguing aspect of extracellular vimentin is its interaction with pathogens during the invasion process. Studies have shown that vimentin can directly bind to viruses and bacteria, influencing whether these pathogens are internalized by host cells. Interestingly, the effect of vimentin varies depending on the pathogen: for example, in SARS-CoV infections, vimentin facilitates viral entry by acting as a docking platform on the cell membrane. In contrast, during human papillomavirus (HPV) infections, it acts as a physical barrier, trapping the virus and slowing its entry into cells. In this study, we investigate the role of extracellular vimentin in modulating pathogen invasion by developing a mathematical model that incorporates five key components: the pathogen, vimentin, the pathogen-vimentin complex, healthy epithelial cells, and infected epithelial cells. Through a combination of analytical tools, such as asymptotic behavior analysis and transient dynamics, we explore the effects of extracellular vimentin under various biological conditions. Our model enables a deeper understanding of how extracellular vimentin may either support or inhibit infection, depending on the nature of the invading pathogen.

1 Introduction

Background and Context

Vimentin and Extracellular Vimentin

Vimentin is a critical protein that belongs to the family of intermediate filaments [1], which are essential structural components of the cytoskeleton within the cytoplasm of cells [2]. Predominantly expressed in mesenchymal cells such as fibroblasts, endothelial cells, and smooth muscle cells [3], vimentin plays a central role in: maintaining cell shape by providing mechanical support and defining the cellular architecture, facilitating cellular movements such as migration and adhesion, contributing to cellular integrity and forming strong, flexible filamentous networks that enhance resilience against mechanical stress [4, 2, 5]. This dynamic and versatile protein is crucial for various physiological processes, including wound healing, development, and immune responses [2].

While vimentin is traditionally associated with its cytoplasmic role, recent research has revealed its presence in the extracellular environment, where it assumes additional functions beyond providing structural support [3, 6, 7, 8, 9]. Extracellular vimentin, which is either secreted or released into the extracellular matrix (ECM), has emerged as a significant player in tissue remodeling, inflammation, and cancer metastasis [9]. Extracellular vimentin generally exists in two primary forms, each with distinct roles: surface-level extracellular vimentin and secreted extracellular vimentin [6, 7].

Surface-level Extracellular Vimentin

Surface-level vimentin refers specifically to the variant of the vimentin protein that is localized on the external surface of the cell membrane, rather than being confined to its typical intracellular, cytoskeletal location. This extracellular or surface-associated form of vimentin plays a crucial and dynamic role in mediating interactions between the cell and its external environment [4, 6]. One of the primary functions of surface vimentin is to act as a receptor or, in some contexts, a co-receptor. Through this role, it facilitates binding and communication with a variety of external molecules, which in turn can significantly influence the behavior and fate of the cell [9].

A notable example of its function is its ability to bind with the Angiotensin-Converting Enzyme 2 $ACE2$, a well-characterized receptor that has garnered substantial attention due to its role in mediating the entry of certain viruses, including SARS-CoV-2, the virus responsible for COVID-19 [3, 7, 10]. In such pathogen-host interactions, surface vimentin acts as an accessory factor that enhances or enables the docking and internalization of viral particles into host cells, thereby contributing to the efficiency and specificity of infection [7].

Beyond its involvement in infectious disease processes, surface-level vimentin also contributes significantly to other essential cellular functions. These include promoting cell adhesion, facilitating directed cell migration, and modulating immune system responses [6, 11]. In the context of cell adhesion and migration, surface vimentin interacts with integrins and extracellular matrix components, helping cells move through tissues during development, wound healing, or in pathological scenarios like metastasis [9, 12]. Its role in immune modulation is equally critical, as it can influence how immune cells recognize and respond to damaged or infected cells [11, 5].

Taken together, the multifunctional nature of surface vimentin underscores its importance not only in maintaining normal physiological functions but also in contributing to disease mechanisms, including cancer progression and infectious diseases [12, 7]. Its diverse roles make it a promising target for therapeutic interventions and a valuable biomarker in both research and clinical settings [13].

Secreted form of Extracellular Vimentin

Secreted vimentin is the form of vimentin fully released into the extracellular matrix (ECM). It functions as an effector protein, binding to receptors on other cells and influencing their activity. For

example, secreted vimentin interacts with the Insulin-like Growth Factor 1 Receptor (IGF-1R) to promote axonal growth, activates immune signaling through Dectin-1, and modulates cell adhesion via CD44. By mediating these diverse interactions, secreted vimentin contributes to processes like tissue remodeling, immune response, and inflammation [9, 11]. Recent research has revealed that, in addition to the conventional endoplasmic reticulum–Golgi secretory pathway, proteins can be exported through alternative mechanisms known as unconventional protein secretion (UPS) pathways. Currently, four types of UPS have been identified. The release of extracellular vimentin by tumor endothelial cells has been linked to type III UPS [6, 11].

This dual role of vimentin as both a structural cytoplasmic component and an extracellular effector highlights its versatility and importance in both physiological and pathological contexts.

Structure and Forms of Vimentin

Gaining a comprehensive understanding of the structural composition of vimentin in both its intracellular and extracellular states is essential for fully grasping its broad spectrum of biological functions across various physiological and pathological contexts. Within the intracellular environment, vimentin undergoes a highly organized, stepwise assembly process shown in Figure 1 from [11]. It begins as individual polypeptide chains, which first associate to form coiled-coil dimers [14]. These dimers then align laterally to generate tetramers, each consisting of two antiparallel, staggered dimers. The next stage in this hierarchical process involves the lateral association of eight tetramers to produce unit-length filaments (ULFs), which are typically around 60 nanometers in length. These ULFs subsequently elongate and anneal in an end-to-end manner, eventually forming intricate and dynamic filamentous networks that comprise the vimentin intermediate filament cytoskeleton [6, 11].

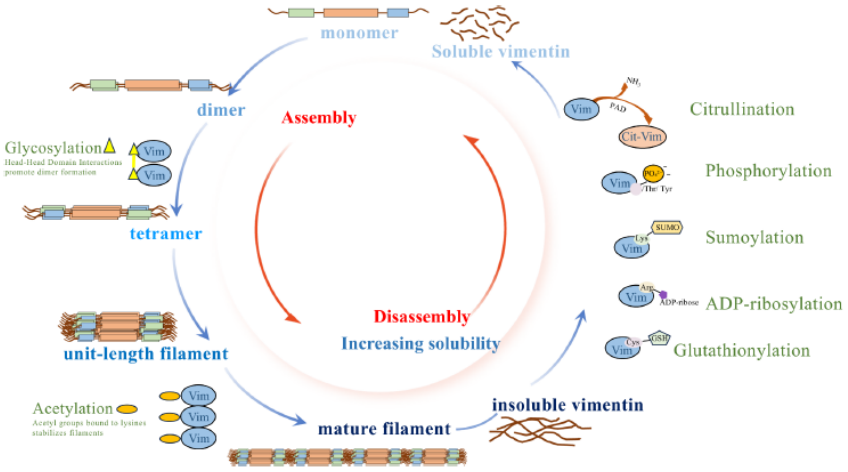

Figure 1: Detailed assembly and disassembly process of different structures of vimentin explained [11].

These filamentous networks are vital for several key cellular functions. They provide critical structural support that helps preserve the cell's overall integrity and mechanical resilience, particularly under conditions of stress or deformation [6]. Moreover, they contribute significantly to the maintenance of cell shape, enabling cells to adapt their morphology during dynamic processes such as migration and division [4]. Vimentin filaments also interact with multiple cellular components, including signaling molecules and organelles, thereby influencing a variety of signaling pathways and intracellular transport mechanisms [11].

Molecularly, vimentin is classified as a type III intermediate filament protein with a molecular weight of approximately 54 kilodaltons. It is composed of a total of 466 amino acids arranged into three primary domains: a central rod-like alpha-helical domain responsible for filament formation, flanked by a non-helical head domain (N-terminal) and a tail domain (C-terminal) [6, 14]. The central alpha-helical coil is pivotal in driving the assembly process, facilitating the formation of stable dimeric and tetrameric structures, while the head and tail domains are believed to regulate filament

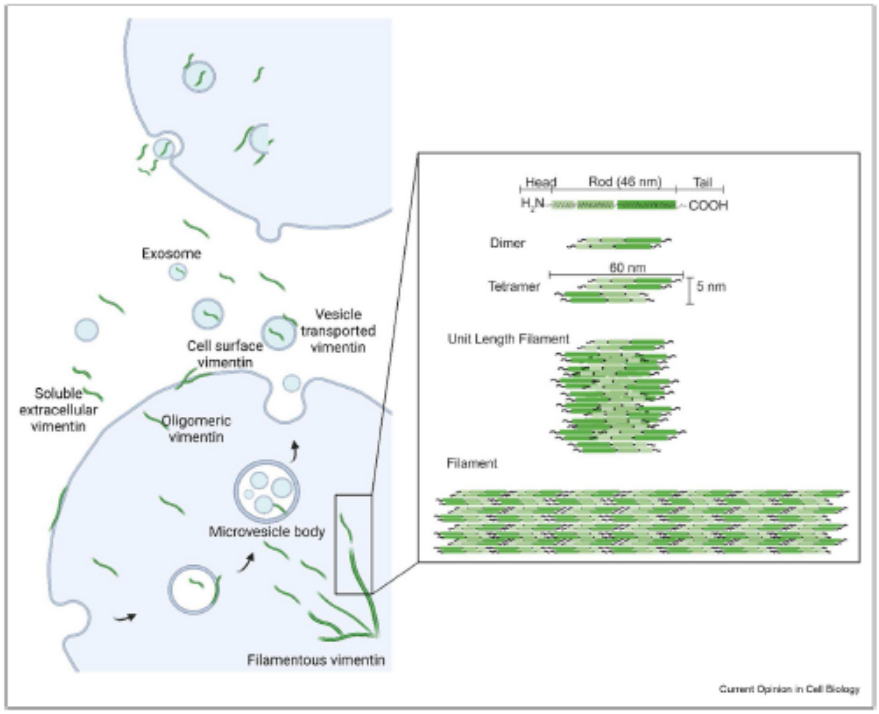

Figure 2: Different structures and forms of vimentin both extracellular and intracellular are simply shown in the schematic diagram [6]

dynamics, interactions with other proteins, and post-translational modifications. This modular design allows vimentin to function flexibly and respond to various intracellular cues, contributing to its role as a dynamic scaffold within the cytoskeleton [6, 11, 14].

In the extracellular environment, vimentin primarily exists in shorter, non-filamentous forms. These extracellular forms may contribute to cell communication and tissue repair, differing significantly from the filamentous networks observed in mesenchymal cells. Vimentin expression is often upregulated in cancer, where it enhances motility and invasiveness, and it serves as a target for certain pathogens. Furthermore, post-translational modifications and isoform variations add complexity to its functions [6].

Extracellular vimentin also exists in soluble and insoluble forms, each with distinct characteristics and functional roles [4]. The different shapes and forms are shown in Figure 2. Soluble vimentin refers to vimentin molecules freely present in the extracellular matrix (ECM) or circulating in bodily fluids, such as blood and lymph. It does not assemble into large filamentous structures and is often found in shorter, non-filamentous forms [14, 11]. Insoluble vimentin exists as filamentous or aggregated structures, typically anchored to the surface of cells or forming part of the ECM. It is more stable and organized compared to its soluble counterpart. Especially, this insoluble form participates in pathogen-host interactions, often acting as a binding partner for pathogens during invasion [11, 6]. The balance between soluble and insoluble extracellular vimentin depends on the local cellular environment and the stimuli received. For instance, during inflammation or tissue damage, soluble vimentin may be secreted to mediate immune and repair processes. Whereas, in cancer or pathogen interactions, insoluble surface vimentin may be upregulated to facilitate adhesion or invasion [6, 4].

Pathogen-Host Dynamics

Here, we are interested in the mechanism of how different pathogens interact with host components during the invasion and more particularly, how extracellular vimentin works in the presence of different pathogens in the immune system. In the presence of pathogens, extracellular vimentin has been found to bind to pathogens, specifically in the case of SARS-CoV-2 [7], the process is illustrated in

Figure 3 visually. Since we are interested in the mechanism of how the pathogen invades and spreads infections in the host body, a summary of all the different interactions and what has been studied so far is presented here:

- **Bacterial interaction**

  Extracellular vimentin plays a significant role in bacterial pathogenesis by functioning as a versatile mediator in host-pathogen interactions. It acts as a receptor or co-receptor on the cell surface, facilitating bacterial adhesion to host tissues. Additionally, vimentin can participate in activating intracellular signaling pathways that promote bacterial entry and invasion. Beyond its involvement in adhesion and invasion, extracellular vimentin also contributes to immune modulation, potentially altering host immune recognition and responses in a way that favors bacterial persistence and survival. Through these mechanisms, bacteria effectively exploit extracellular vimentin to enhance their infectivity and evade host defenses [6, 12, 4].

  In cases of bacterial meningitis caused by E. coli K1, the bacteria utilize their virulence factor IbeA to bind to surface vimentin on brain microvascular endothelial cells [12]. This interaction activates signaling pathways required for the bacteria to invade these cells. Also, the surface-level vimentin acts as a receptor that senses matrix stiffness and facilitates the invasion of human microvascular endothelial cells (HMEC-1) [6, 15].

  In the context of gastrointestinal infections caused by Escherichia coli, particularly adherent-invasive E. coli (AIEC), vimentin exhibits a dual functionality. On the cell surface, it acts as a receptor that facilitates the recognition and attachment of AIEC to host cells, promoting bacterial colonization. Intracellularly, vimentin serves as a pattern recognition receptor (PRR), capable of detecting bacterial components such as peptidoglycan fragments. This recognition initiates innate immune responses, contributing to the host's defense mechanisms against infection [6].

  Meningitis caused by Streptococcus agalactiae, surface vimentin on host cells plays a key role by interacting with the bacterial surface protein BspC [6, 4]. This binding facilitates the adherence of the bacteria to brain endothelial cells, a critical step in crossing the blood-brain barrier. The interaction not only promotes bacterial colonization but also triggers inflammatory responses that contribute significantly to the onset and progression of the disease [13].

  In monocytes infected with Mycobacterium tuberculosis, vimentin is expressed on the cell surface and acts as a ligand for the NKp46 receptor on natural killer (NK) cells [4]. This interaction facilitates the targeting and destruction of infected monocytes by NK cells. When specific antibodies block vimentin, NK cells are less effective at lysing infected monocytes, impairing immune defense. Pathogens like Salmonella enterica and Chlamydia trachomatis recruit and remodel intracellular or surface vimentin to their advantage [6]. These modifications help pathogen binding, invasion, and the modulation of innate immune signaling to favor bacterial survival and replication [15].

- **Viral interaction**

  Extracellular vimentin plays a multifaceted role in viral infections by assisting viruses with diverse genome types, such as DNA, single-stranded RNA, and double-stranded RNA, in invading host cells. It can function as a primary receptor, a co-receptor, or even as a restriction factor depending on the virus [6, 15]. Both extracellular and intracellular forms of vimentin contribute to key stages of the viral life cycle, including entry, replication, and release. Interestingly, while it facilitates infection for many viruses, vimentin can also inhibit others, such as human papillomavirus (HPV) [6, 9, 8], highlighting its complex and dualistic nature. This versatility makes vimentin a promising target for developing antiviral therapies [16].

  In the case of SARS-CoV and SARS-CoV-2 (COVID-19), extracellular vimentin interacts with the virus's spike protein, helping it dock on host cells and facilitating entry [15, 6, 4, 9]. It has

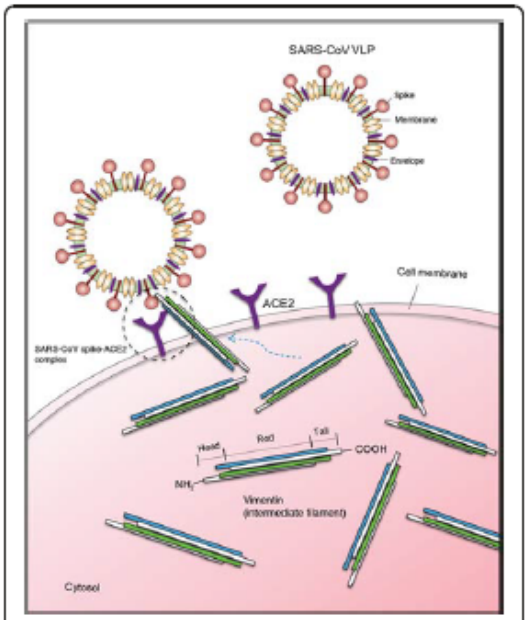

Figure 3: The figure from [7] visually illustrates how SARS-CoV pathogens spike protein attach to the ACE2 receptor in the cell surface for internalization.

been found to form a docking platform with ACE2, the main receptor for SARS-CoV-2 [3, 7, 10]. Various recent studies have also shown that blocking vimentin with antibodies can prevent the virus from entering cells [13].

Vimentin also facilitates the attachment and invasion of various viruses, including Chandipura virus, Japanese encephalitis virus, porcine reproductive and respiratory syndrome virus, cowpea mosaic virus, and dengue virus (DENV) [6]. For example, DENV directly binds to the rod domain of surface vimentin on endothelial cells to initiate infection. Similarly, Enterovirus 71 targets the N-terminal region of surface vimentin as an attachment site and can even upregulate vimentin expression on the host cell surface to enhance its infectivity [16]. These interactions underscore vimentin's critical role in the viral entry process across a broad range of pathogens.

On the other hand, Vimentin can act as a restriction factor for HPV, limiting its internalization into host cells [4, 6, 16]. Surface and soluble vimentin hinder HPV entry through physical barriers or steric hindrance. Reducing vimentin increases HPV infection, while increasing vimentin reduces it. Due to its important role in viral disease progression, like in Zika virus, influenza A virus, and Parainfluenza virus, targeting vimentin in the therapeutic process with small molecules can disrupt virus-related processes like endocytosis and trafficking [6]. In conditions like SARS-CoV-2 infection, it may reduce lung injury and fibrosis.

- **Cancer cell interaction**

  Extracellular vimentin plays a significant and multifaceted role in the progression and metastasis of cancer by engaging in complex interactions with both the tumor microenvironment and the cancer cells themselves [16]. When expressed on the cell surface, vimentin functions as a receptor or co-receptor, modulating key intracellular signaling cascades that drive tumor cell proliferation, migration, and invasive behavior. Its presence within the extracellular matrix further contributes to the remodeling of the surrounding tissue architecture, effectively creating a permissive environment for cancer cells to breach tissue boundaries, infiltrate adjacent regions, and ultimately gain access to the circulatory system, facilitating metastasis [4, 17].

  In addition to these structural and signaling functions, extracellular vimentin is also involved in the process of angiogenesis—the formation of new blood vessels—which is vital for sus-

taining tumor growth. It promotes the adhesion and guided migration of endothelial cells, enabling the vascular network expansion required to supply nutrients and oxygen to the tumor mass. Furthermore, emerging research indicates that extracellular vimentin can interact directly with specific molecules on the surface of cancer cells, aiding in their ability to evade immune detection and enhancing their metastatic capabilities. These diverse and dynamic roles underscore the importance of extracellular vimentin as a central regulator of cancer cell behavior and position it as a promising target for therapeutic intervention aimed at limiting tumor progression and spread[17].

Understanding these extracellular vimentin and pathogen interactions is crucial for knowing important mechanisms and factors for disease progression, as well as advancing therapeutic interventions. In addition, these studies show potential applications of extracellular vimentin in drug development or vaccine design [13]. However, for this study, we will not be exploring the therapeutic aspects, instead, we focus on understanding the pathogen invasion and disease progression process only.

Research Gaps and Motivation

Studying vimentin is vital not only for basic biological research but also for its potential clinical applications and for deepening our understanding of various disease mechanisms. As a key structural component of the intermediate filament network, vimentin plays a fundamental role in maintaining cellular integrity, providing mechanical support, and preserving cell shape under both normal and stress conditions [5]. Investigating vimentin allows researchers to explore how intermediate filaments contribute to the organization and resilience of the cytoskeleton. Moreover, understanding the detailed process of vimentin assembly from individual monomers to dimers, tetramers, and ultimately mature filaments sheds light on the broader mechanisms of intermediate filament formation, which is essential for numerous cellular processes, including motility, signaling, and division. This knowledge forms a foundation for exploring how disruptions in cytoskeletal dynamics can contribute to pathological states such as cancer, infection, and degenerative diseases [13].

Overall, studying vimentin offers a comprehensive view of its crucial roles not only in cellular mechanics but also in disease pathology and potential therapeutic applications. It helps in studies of disease mechanisms like cancer and neurodegenerative diseases. Vimentin is used as a biomarker for certain cancers and other diseases [17]. Research can improve diagnostic tools and help in the early detection of diseases. Understanding vimentin's role in disease processes may lead to the development of targeted therapies that specifically disrupt its function in pathological conditions [3, 16].

Despite extensive research into the functions of extracellular vimentin in both normal physiology and disease states, there are still considerable gaps in our understanding of its precise molecular mechanisms, especially in the contexts of pathogen invasion and immune modulation. While numerous studies have highlighted its interactions with bacteria, viruses, and cancer cells, a comprehensive and unified view of how extracellular vimentin operates across these different biological scenarios is still lacking. For instance, although it is known to facilitate bacterial adhesion and invasion, the exact signaling pathways and downstream effects triggered by its engagement with microbial components remain poorly defined. Similarly, in viral infections, the mechanisms by which extracellular vimentin acts as a receptor or co-receptor, and the implications of these interactions for viral replication and immune evasion, are not yet fully understood. In cancer, although its role in promoting metastasis and aiding immune escape has been documented, its broader influence on tumor microenvironment remodeling, including effects on stromal and immune cells, requires deeper exploration. Addressing these knowledge gaps is essential for fully realizing the potential of extracellular vimentin as a biomarker and therapeutic target across a range of diseases.

From a systems biology perspective, most existing studies focus on qualitative descriptions of these interactions, with little emphasis on quantitative modeling. The absence of robust mathematical frameworks makes it more challenging to predict vimentin's behavior under various pathological conditions or assess potential therapeutic interventions. The lack of integrated experimental

and computational studies presents a significant challenge in translating basic research findings into clinical applications.

Motivated by the notable gap in integrating biological research with mathematical modeling in the study of extracellular vimentin, this research aims to explore the dynamic roles of extracellular vimentin in pathogen invasion and immune modulation through an interdisciplinary approach. Specifically, the study focuses on its interactions with viral pathogens, aiming to develop a framework that combines biological evidence with quantitative modeling. This integrative perspective seeks to bridge the current disconnect between empirical observations and theoretical analysis, offering a more comprehensive understanding of how extracellular vimentin contributes to infection processes and immune responses. Ultimately, the insights gained could lay the groundwork for the development of novel therapeutic strategies that target extracellular vimentin in the treatment of infectious diseases.

Objectives of the Study

The primary aim of this study is to explore the dynamic process of pathogen invasion within the host, with a specific focus on the role of extracellular vimentin within the extracellular matrix (ECM) environment. Although both bacterial and viral pathogens utilize distinct mechanisms to interact with host cells, this research concentrates exclusively on viral invasion. As highlighted in the pathogen-host dynamics discussion, extracellular vimentin significantly contributes to the binding and internalization of viral particles at the cell surface, acting as a facilitator or, in some cases, a regulator that may modulate the pace and outcome of infection. These molecular interactions influence not only the initial stages of viral entry but also the broader trajectory of infection development.

To investigate these mechanisms, the study reviews relevant literature to gather biological insights and constructs a mathematical framework capable of analyzing viral invasion dynamics. Through both analytical and numerical methods, the model incorporates experimental data where available to simulate various infection scenarios and assess the influence of extracellular vimentin on disease progression. By identifying key parameters and patterns, this interdisciplinary approach seeks to unify biological understanding with computational analysis, offering a more robust perspective on the multifaceted role of extracellular vimentin in viral pathogenesis. Ultimately, the findings are intended to serve as a foundation for future research that combines mathematical tools with biological exploration to better understand and potentially control infectious diseases.

Significance of Mathematical Modeling and Application to Extracellular Vimentin

Mathematical modeling has emerged as a vital approach in modern biology, offering a powerful means to translate the complexity of biological systems into structured, quantifiable representations. Many biological processes, ranging from intracellular molecular interactions to large-scale physiological or ecological systems, are governed by highly interconnected and nonlinear dynamics that are often difficult to decipher through experimental observation alone. By constructing mathematical models, researchers can simulate these processes, test hypotheses, and explore various scenarios under controlled conditions. These models not only help in identifying key regulatory components and feedback loops but also allow for the prediction of system behavior under different perturbations, thereby providing valuable insights that complement experimental findings and drive further scientific discovery.

In the context of infectious diseases, mathematical models serve as essential tools for simulating complex pathogen-host interactions, forecasting disease progression, and assessing the potential efficacy of interventions such as antiviral drugs, vaccines, or public health measures. These models enable researchers to test biological hypotheses in silico, optimize experimental and clinical study designs, and pinpoint critical parameters that influence infection dynamics, such as viral replication rates, immune response strength, or host susceptibility. Furthermore, mathematical modeling facilitates the exploration of both temporal and spatial dynamics, shedding light on how localized

changes, such as viral entry at a specific site, can propagate through the host system or population. This ability to integrate multiple layers of biological complexity makes modeling a powerful complement to experimental research, enhancing our understanding of infectious processes and informing evidence-based decision-making in disease control.

One of the key strengths of mathematical modeling lies in its ability to bridge biological processes across multiple scales. From microscopic events, such as molecular interactions, protein binding, and intracellular signaling pathways, to macroscopic phenomena like tissue-level responses or population-scale epidemic dynamics, models provide a unified framework for analyzing and linking these diverse levels of organization. This cross-scale integration is especially valuable in studying complex biological systems, such as the role of extracellular vimentin in pathogen invasion, where localized molecular interactions can have far-reaching effects on cellular behavior, tissue integrity, and overall disease progression. By capturing these interconnected layers within a coherent mathematical structure, modeling offers a holistic perspective that enhances both mechanistic understanding and predictive power.

Researchers can refine theoretical predictions, uncover emergent properties, and identify novel therapeutic strategies by coupling experimental data with mathematical frameworks. The iterative feedback loop between modeling and experimentation enhances our ability to address fundamental questions in biology while informing practical applications in medicine, biotechnology, and public health. As biology becomes increasingly quantitative, mathematical modeling is pivotal in advancing our understanding of life and disease.

In this study, we start by developing a mathematical model that integrates the knowledge gathered from an extensive review of the existing literature, carefully selecting the most relevant factors and parameters that govern the process of pathogen invasion, particularly focusing on the role of extracellular vimentin. Once the model is established, we perform a detailed mathematical analysis to determine all possible equilibrium states of the system and examine their stability, which provides critical insights into the long-term behavior of the infection dynamics. Given the scarcity of experimental studies and quantitative data in this specific area, our ability to conduct comprehensive numerical simulations is limited. However, by utilizing the constructed framework, we simulate a variety of infectious scenarios using available data and well-founded parameter estimations. This numerical exploration allows us to better understand the influence of key parameters, highlighting which factors most significantly affect infection progression and offering a foundation for refining future experimental and theoretical research in this field.

2 The Main Model:

2.1 Conceptual Consideration

For the formulation of the mathematical model, we have the following key points in our consideration:

Questions to answer in the study:

Role of extracellular vimentin in viral pathogen invasion within a host along with the dynamical changes in pathogen population, extracellular vimentin population, and epithelial cell population.

Key Biological Mechanisms Considered:

- Pathogen Dynamics:
  - Pathogens invade host cells, utilize cellular DNA or RNA for replication, and proliferate [13].
  - In HPV, extracellular vimentin acts as a delaying factor, limiting internalization into host cells [6].
  - For viruses like SARS-CoV, Chandipura, DENV, and Japanese encephalitis, vimentin facilitates cell invasion [6, 4].
- Host Immune Response:
  - Pathogens can be removed by the host's innate immune system [3].
  - Soluble extracellular vimentin-bound pathogens can be cleared by phagocytosis via macrophages, neutrophils, or dendritic cells [18].
- Extracellular Vimentin Dynamics:
  - Vimentin can be released in the extracellular matrix in response to the immune action by cells like Macrophages, exosomes, neutrophils, etc [13].
  - Extracellular vimentin (both cell surface and secreted) binds with pathogens to form a pathogen-vimentin complex (P-V complex) before cell entry [7, 6, 4, 3, 12].
  - Regulation process, including autocrine signaling [2], activation [6], secretion [6], and removal [2], is also considered.
- Cellular Interactions:
  - Pathogens bound to surface vimentin are internalized into host cells [6].
  - Internalized pathogens use intracellular cytoplasmic vimentin for trafficking towards the nucleus [12], leading to infected cells.
- Epithelial Cell Dynamics:
  - Healthy and infected epithelial cells are the primary cell types considered.
  - Infected epithelial cells can undergo apoptosis or lysis, releasing pathogens into the extracellular matrix (ECM) for further invasion [19].
  - Epithelial cells represent the membranes of organs such as the lungs and respiratory system.
- Pathogen Lifecycle:
  - Replicated pathogens are released into the ECM following the apoptosis or lysis of infected cells, enabling reinfection of other cells [19, 13].

2.2 Formulation:

To formulate the main framework for the pathogen invasion model here, we consider the pathogen as the variable P, the activated extracellular vimentin as V, the pathogen-vimentin complex as P_V, the host cell H and the infected cell variable I.

The following mathematical model is the proposed model for the study here:

$$\begin{aligned}
\frac{dP}{dt} &= -\lambda PV + (\delta_1+\delta_2)\pi I + k\pi I(H+I) - \rho_1 P \\
\frac{dV}{dt} &= -\lambda PV + \gamma VH + f(P) + g(P,H,I) - \rho_2 V \\
\frac{dP_v}{dt} &= \lambda PV - \sigma P_v H - \rho_M P_v \\
\frac{dH}{dt} &= -\sigma P_v H + (b-\delta_1)H - kH(H+I) \\
\frac{dI}{dt} &= \sigma P_v H - \delta_2 I + (b-\delta_1)I - kI(H+I)
\end{aligned} \tag{1}$$

with the initial conditions,

$$P(0) = p_0, V(0) = v_0, P_v(0) = p_{v_0}, H(0) = h_0, I(0) = i_0.$$

Here, all the parameters and the initial values are non-negative. The model is also shown in diagram form in Figure 4. Next, we describe all the differential equations formulated here with all the parameter representations.

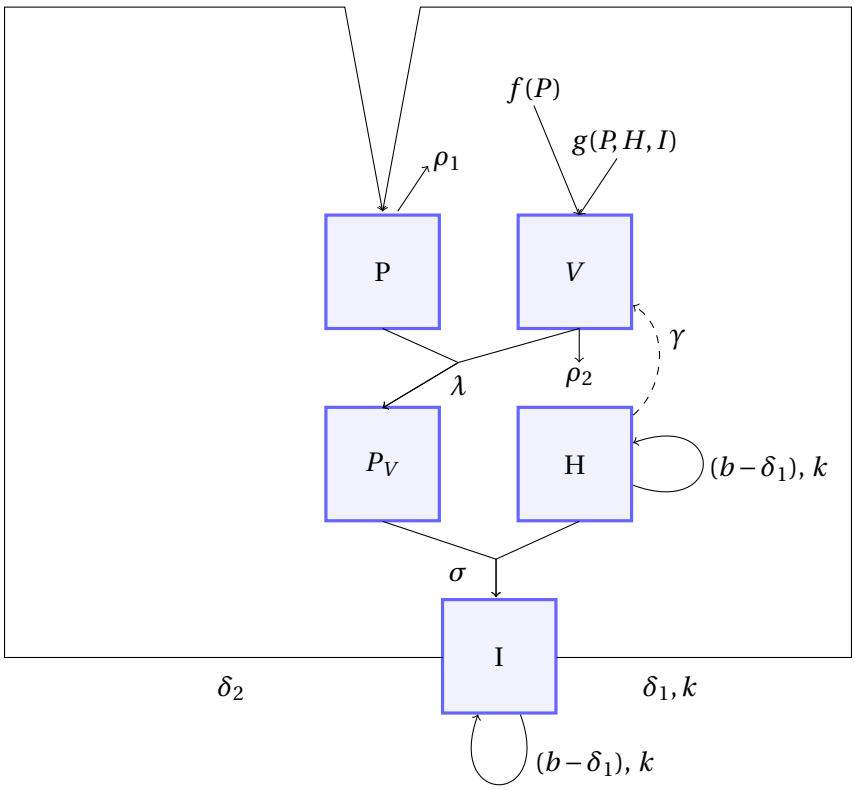

Figure 4: The diagram of the model.

2.3 Description:

For the dynamics of the pathogen ($\frac{dP}{dt}$) inside the host, $-\lambda PV_E$ term describes that the pathogens P interact with the activated extracellular vimentin V and bind with them at λ rate to create Pathogen-

Vimentin complex (P-V complex). Then, $\delta_2 \pi I$ term in the pathogen dynamics represents that pathogens are being produced inside the host cell at π rate, and then due to the lysis of the infected cell at δ_2 rate they are being released in the extracellular environment. Whereas, the other terms $\delta_1 \pi I + k\pi I(H+I)$ show the increment of pathogens inside the host cells in a similar way, and due to the apoptosis of the infected epithelial cells at δ_1 rate they are being released. Also, k is the competition rate of the cells and can cause natural death to the infected epithelial cells causing pathogens to be released outside.

Then in the dynamics of the extracellular vimentin ($\frac{dV}{dt}$), we also notice the term $-\lambda P V_E$ representing the loss of extracellular vimentin while binding with the pathogens. The functions $f(P)$ describe the secretion of the extracellular vimentin proteins in the presence of pathogens inside the body. Here, we assume the expression of these functions as, $f(P) = \beta_2 P$. The function $g(P,H,I)$ is used to describe more extracellular vimentin activation rate due to inflammation signals and the expression is, $g(P,H,I) = \beta_1 P(H+I)$. Also, the term $\gamma V H$ represents the activation of more vimentin through autocrine signaling from the host cells, where γ is the autocrine rate. Lastly, the term $-\rho_2 V$ represents the removal of vimentin as a process of the regulations.

Next, in the equation describing the dynamics of the P-V complex ($\frac{dP_v}{dt}$), we observe the positive term, $\lambda P V$ describes the formation of these complex forms of pathogen and proteins due to interaction between them. Then the internalization of the P-V complex P_v inside the host cell H at σ rate is described using $-\sigma P_v H$ term. The last term of this equation $-\rho_M P_v$ is used to describe the trapping process of the P-V complex by the immune system of the body.

The host cell dynamics ($\frac{dH}{dt}$), shows the internalization process of pseudovirus P_v inside host cell H causing the host cell to turn into the infected cell by the term $-\sigma P_v H$. The last part $(b-\delta_1)H - kH(H+I)$ depicts the proliferation of the host cells, where b is the cell growth rate, δ_1 is the normal cell death rate, k is the carrying capacity of the cells.

Finally, in the $\frac{dI}{dt}$ equation, $\sigma P_v H$ is simply the term explaining how we get the infected cells by internalization process. Then the term $-\delta_2 I$ shows how we lose infected cells because of the lysis of these cells and $(b-\delta_1)I - kH(H+I)$ is the normal proliferation of the infected cells just like the host cells.

The description of the model is summarized in the diagram 5.

3 Analysis of Model (1):

Now, from the derived model in (1) we have the final form as follows:

$$\begin{aligned}
\frac{dP}{dt} &= -\lambda P V + (\delta_1+\delta_2)\pi I + k\pi I(H+I) - \rho_1 P = F_1(P,V,P_v,H,I)\\
\frac{dV}{dt} &= -\lambda P V + \gamma V H + \beta_2 P + \beta_1 P(H+I) - \rho_2 V = F_2(P,V,P_v,H,I)\\
\frac{dP_v}{dt} &= \lambda P V - \sigma P_v H - \rho_M P_v = F_3(P,V,P_v,H,I)\\
\frac{dH}{dt} &= -\sigma P_v H + (b-\delta_1)H - kH(H+I) = F_4(P,V,P_v,H,I)\\
\frac{dI}{dt} &= \sigma P_v H - \delta_2 I + (b-\delta_1)I - kI(H+I) = F_5(P,V,P_v,H,I)
\end{aligned} \tag{2}$$

with the initial conditions,

$$P(0) = p_0, V(0) = v_0, P_v(0) = p_{v_0}, H(0) = h_0, I(0) = i_0.$$

3.1 Wellposedness :

To describe wellposedness of the model (2), we observe F_1, F_2, F_3, F_4 and F_5 in the equations of (2), and they are polynomials depending on the dependent variables (P,V,P_v,H,I) only. Therefore, the

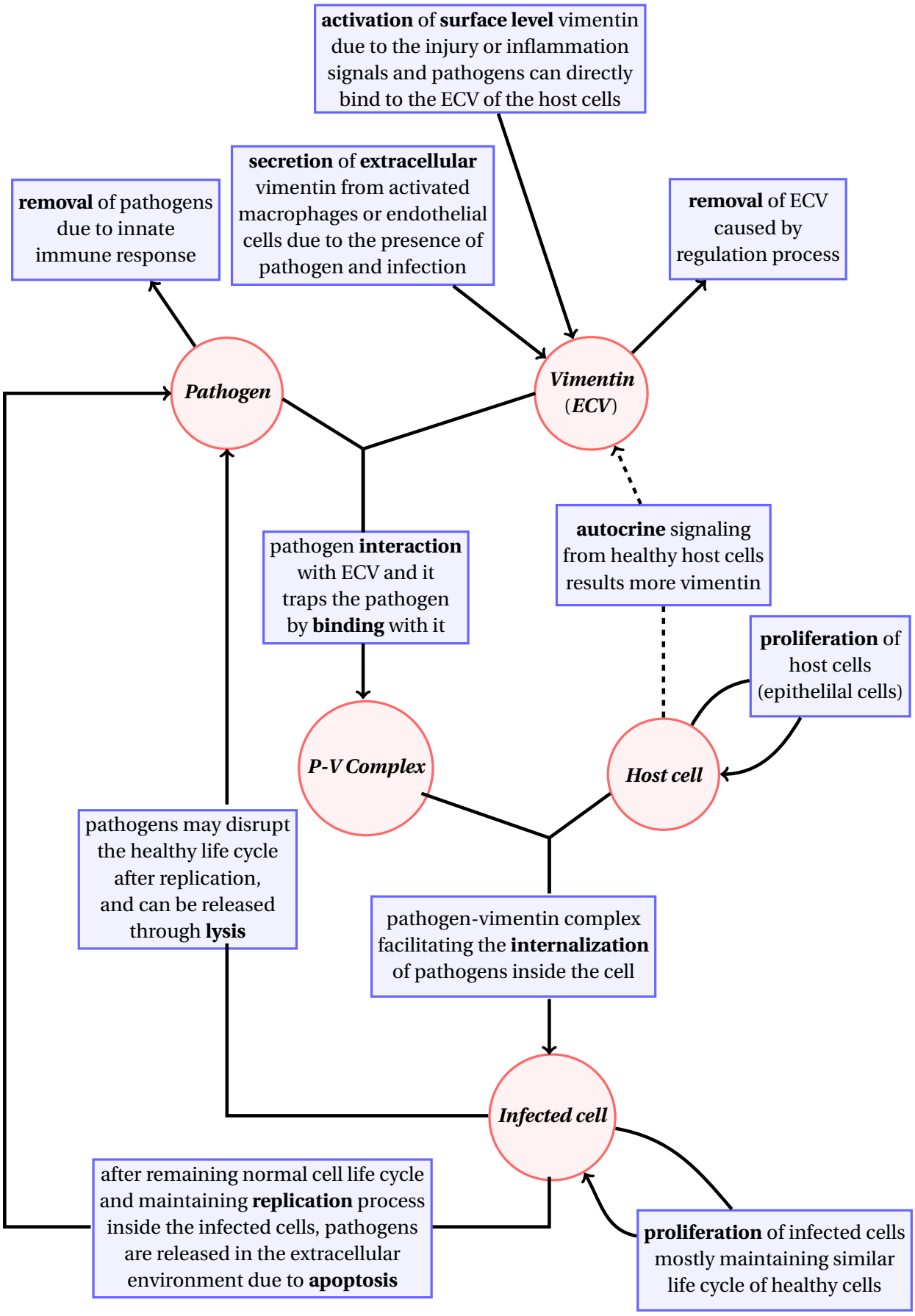

Figure 5: Biological description and consideration are briefly explained in the diagram.

system is autonomous. Also, since the functions F_1, F_2, F_3, F_4 and F_5 are continuously differentiable everywhere on $\mathbb{R}^5_+$ with respect to variables, the system of equations described in the model (2) has existence of solutions as well as there are uniqueness of the solutions for the given initial conditions on the interval.

Also, for the non-negativity of the solutions of the given model in (2), we note that all parameters and initial conditions are taken from non-negative intervals. At any point where a state variable (P, V, P_v, H, I) reaches zero, the corresponding differential equation satisfies $F_X(\cdots, X = 0, \cdots) \geq 0$ and often strictly > 0, due to the structure of the model. This implies that the vector field points inward at the boundary of the positive quadrant, preventing trajectories from leaving the non-negative region. For strictly positive initial conditions, the solutions remain strictly positive and bounded away from zero. Thus, proving that the system is always positively invariant. Therefore, the system's solutions are always non-negative. Hence, the system is well-posed.

Since the system described for the study is well-posed, we can calculate the equilibrium solutions to analyze the model behaviour further here.

3.2 Computation of Equilibria and their Stability:

In the study of dynamical systems, we often study the equilibrium solutions or steady states of the system to understand the system's long-term behaviour. Also, studying the equilibria can be effective in understanding how the system may behave under different parameter restrictions and conditions. In addition to that, it is easier to analyze a complicated dynamical system using this technique, especially when the system is a high-order system, and the exact solution is very complex to derive. Moreover, in this study, we are interested in investigating the equilibrium solutions to observe the extracellular vimentin's role in the infectious events, and we also aim that our study will reflect some strategies, which we can easily do with these analytical computations. Here, we compute the equilibrium solutions of the model (2) and analyze their stability.

Zero Equilibrium

In (2), $(P, V, P_v, H, I) = (0, 0, 0, 0, 0)$ is a solution of the model, while we assume the system is in equilibrium, i.e, the right-hand side of the equations are zero. So, zero is an equilibrium of the system.

The zero equilibrium here represents that all the variables of the system vanish. Biologically, this would mean that the pathogen, extracellular vimentin, pathogen-vimentin complex, and all the epithelial cells, including healthy and infectious ones extinct, which inside a host body of a living organism is not feasible.

Boundary Equilibrium

Let $(P, V, P_v, H, I) = (0, 0, 0, h_e, 0)$ be a equilibrium of the model (1) where we consider $h_e \neq 0$ and if we solve, $\frac{dH}{dt} = 0$ in this case,

$$h_e[b - \delta_1 - kh_e] = 0$$

we get $h_e = \frac{b-\delta_1}{k}$ and $(0, 0, 0, \frac{b-\delta_1}{k}, 0)$ as an equilibrium for model (2). This equilibrium shows that only the healthy epithelial cell dynamics are present in the system, while the other components, like pathogens and infected cells, are inactive. In addition to that, the existence condition of the boundary equilibrium here is,

$$b - \delta_1 > 0.$$

The existence condition shows that at the equilibrium, the system will proliferate healthy epithelial cells and stabilize the dynamics with no pathogen or infection being functional in the long run. Also, the extracellular vimentin's role is inactive in the system as well. However, we are not interested in exploring this situation in this study.

Stability of the Zero Equilibrium:

Now, to analyze the stability of the equilibrium, we use the Jacobian, where the **Jacobian of the model** (2) has the following form:

$$J = \begin{bmatrix} -\lambda V-\rho 1 & -\lambda P & 0 & k\pi I & \delta_1\pi+k\pi H+2k\pi I+\delta_2\pi \\ -\lambda V+\beta_2+\beta_1(H+I) & -\lambda P+\gamma H-\rho_2 & 0 & \gamma V+\beta_1 P & \beta_1 P \\ \lambda V & \lambda P & -\sigma_1 H-\rho_M & -\sigma_1 P_v & 0 \\ 0 & 0 & -\sigma_1 H & -\sigma_1 P_v+b-\delta_1-2kH-kI & -kH \\ 0 & 0 & \sigma_1 H & \sigma_1 P_v-kI & -\delta_2+(b-\delta_1)-kH-2kI \end{bmatrix} \tag{3}$$

Now, we calculate the Jacobian J_0 by plugging in $(P,V,P_v,H,I) = (0,0,0,0,0)$ in the (3) matrix, we get,

$$J_0 = \begin{bmatrix} -\rho 1 & 0 & 0 & 0 & (\delta_1+\delta_2)\pi \\ \beta_2 & -\rho_2 & 0 & 0 & 0 \\ 0 & 0 & -\rho_M & 0 & 0 \\ 0 & 0 & 0 & b-\delta_1 & 0 \\ 0 & 0 & 0 & 0 & b-\delta_1-\delta_2 \end{bmatrix}$$

So, the characteristic equation for the Jacobian matrix here is,

$$P_{(0,0,0,0,0)}(\Lambda) = 0 \Rightarrow (-\rho_1-\Lambda)(-\rho_2-\Lambda)(\rho_M-\Lambda)(b-\delta_1-\Lambda)(b-\delta_1-\delta_2-\Lambda) = 0$$

and numerating the eigenvalues we find,

$$\begin{aligned} \Lambda_1 &= -\rho_1 \\ \Lambda_2 &= -\rho_2 \\ \Lambda_3 &= -\rho_M \\ \Lambda_4 &= b-\delta_1 \\ \Lambda_5 &= b-\delta_1-\delta_2 \end{aligned}$$

Since $\Lambda_1, \Lambda_2, \Lambda_3 \leq 0$, then we can say that the zero equilibrium is locally asymptotically stable if $b < \delta_1$ and $b < \delta_1+\delta_2$, otherwise, the equilibrium is unstable. Observing both of the stability conditions, we can combine them and say that the stability condition for the zero equilibrium is $b < \delta_1+\delta_2$.

Since, from the stability condition, b, the growth rate of epithelial cells needs to be smaller than the natural death rate of the cells, in the long run, the system will be completely out of epithelial cells since the cell population cannot be stabilized under the predictions here. Also, a similar interpretation we have from the other stability condition, where it shows that the growth rate is smaller than the normal and infectious death rate of the cells. Therefore, the system completely goes towards zero, making all the components extinct here, which is not a practical scenario inside a living organism, even though the system is pathogen and infection-free. It can only be a feasible situation if the system is in a lab testing environment or a petri dish. Thus, inside a host body, we need $b > \delta_1$ for the epithelial cells to survive.

Stability of the Boundary Equilibrium:

Similar to the previous equilibrium, we now calculate the Jacobian matrix at the boundary equilibrium using the Jacobian mentioned in (3),

$$J_{h_e} = \begin{bmatrix} -\rho_1 & 0 & 0 & 0 & \delta_1\pi+\delta_2\pi+2k\pi h_e \\ \beta_2+\beta_1 h_e & -\rho_2+\gamma h_e & 0 & 0 & 0 \\ 0 & 0 & -\rho_M-\sigma_1 h_e & 0 & 0 \\ 0 & 0 & -\sigma_1 h_e & b-\delta_1-2kh_e & -kh_e \\ 0 & 0 & \sigma_1 h_e & 0 & -\delta_2+b-\delta_1-kh_e \end{bmatrix}$$

The characteristic polynomial has the following form:

$$P_{h_e}(\Lambda) = (-\rho_1)(-\rho_2 + \gamma h_e)(-\rho_M - \sigma_1 h_e)(b - \delta_1 - 2kh_e)(-\delta_2 + b - \delta_1 - kh_e) = 0$$
$$\Rightarrow (-\rho_1)(-\rho_2 + \frac{\gamma}{k}(b - \delta_1))(-\rho_M - \frac{\sigma_1}{k}(b - \delta_1))(-b + \delta_1)(-\delta_2) = 0$$

Then, calculating the eigenvalues using the characteristic equation, we get,

$$\begin{aligned}
\Lambda_1 &= -\rho_1 \\
\Lambda_2 &= -\rho_2 + \frac{\gamma}{k}(b - \delta_1) \\
\Lambda_3 &= -\rho_M - \frac{\sigma_1}{k}(b - \delta_1) \\
\Lambda_4 &= -b + \delta_1 \\
\Lambda_5 &= -\delta_2
\end{aligned}$$

Again, we see that $\Lambda_1, \Lambda_5 \leq 0$. Also, by the existence condition of the boundary equilibrium, Λ_3 and Λ_4 are negative. Hence, the stability condition for this equilibrium is that the equilibrium $(0, 0, 0, \frac{b-\delta_1}{k}, 0)$ is locally asymptotically stable if $\frac{\rho_2}{\gamma} > \frac{(b-\delta_1)}{k}$. This condition interprets that the ratio of the removal rate and autocrine signaling rate of vimentin needs to be higher than the proliferation rate of the healthy cells for the equilibrium to be stable.

Other Equilibria

Even though there are other positive equilibrium solutions of the system exist but calculating the exact expression of other equilibria where we assume (P, V, P_v, H, I) are all non-zero variables is extremely complex. Also, analyzing their stability is not very constructive.

So, we perform an aggregation of variables to reduce the dimension of the model (1) in the next section to find a lower-dimensional dynamical system and to explore the system more functionally.

4 Aggregation of the Model:

Aggregation is a reduction process of complex, high-dimensional mathematical models. It can be performed by combining variables, or sometimes by joining two similar equations through some physical assumptions. It is a common technique used in mathematical analysis to focus on significant dynamical changes only, as well as reducing the computational complexity. The strategy always provides a deeper analysis of the dynamics.

The aim of using this technique here is to reduce the dimension of the system, focus on essential variables, and analyze them more thoroughly. In this process, we reduce the 5-equation dynamical system into a 4-variable and 4-equation system. Here are the detailed assumptions and conditions explained in the aggregation process.

Assumptions and Formulation:

To reduce the dimension of the model (2), we aggregate the equations governing the non-infected and infected epithelial cells - $H(t)$ and $I(t)$ - using the following observation:

$$\begin{aligned}
&\frac{dH}{dt}+\frac{dI}{dt}=(b-\delta_1)(H+I)-k(H+I)^2-\delta_2 I\\
\Rightarrow&\frac{dH}{dt}+\frac{dI}{dt}\leq(b-\delta_1)(H+I)-k(H+I)^2 \quad \text{where,} \quad \delta_2 I\geq 0\\
\Rightarrow&\frac{dH}{dt}+\frac{dI}{dt}\leq\frac{dC}{dt}=(b-\delta_1)C-kC^2=(b-\delta_1)C\left(1+\frac{C}{\frac{b-\delta_1}{k}}\right)
\end{aligned}$$

where the new state variable $C(t)=H(t)+I(t)$ is the total number of epithelial cells, and the carrying capacity of the epithelial cells from the cell dynamic equation here is $K_c=\frac{b-\delta_1}{k}$, where $b-\delta_1>0$. Also, previously, from the zero equilibrium stability of model (2), we noticed how the system becomes completely extinct and the epithelial cells die out as well. Thus, the system is only sustainable if $b-\delta_1>0$. Now, by assumption, let $h_0+i_0\leq K_c$, so

$$H(t)+I(t)\leq K_c, \quad t\geq 0 \tag{4}$$

and at equilibrium $\lim_{t\to\infty}C(t)=K_c$. Hence, for simplification, we assume that the total number of epithelial cells is constant over time, $H(t)=K_c-I(t)$, for $t\geq 0$. So, using $H(t)=K_c-I(t)$ and $K_c=\frac{b-\delta_1}{k}$ in the main model (2) and simplifying it, we have the following form of **the aggregated system**:

$$\begin{aligned}
\frac{dP}{dt}&=-\lambda PV+\delta_2\pi I-\rho_1 P=f_1(P,V,P_v,I)\\
\frac{dV}{dt}&=-\lambda PV+\gamma V(K_c-I)+\beta_2 P+\beta_1 PK_c-\rho_2 V=f_2(P,V,P_v,I)\\
\frac{dP_v}{dt}&=\lambda PV-\sigma_1 P_v(K_c-I)-\rho_M P_v=f_3(P,V,P_v,I)\\
\frac{dI}{dt}&=\sigma_1 P_v(K_c-I)-\delta_2 I=f_4(P,V,P_v,I)
\end{aligned} \tag{5}$$

with the initial conditions, $P(0)=p_0$, $V(0)=v_0$, $P_v(0)=p_{v_0}$, $I(0)=i_0$. Also, we have $i_0=K_c-h_0$ and all the parameters and the initial values p_0, v_0, p_{v_0}, h_0 and $i_0\geq 0$ always.

Here, the model follows the same descriptions as the previous model, and all the terms have similar explanations. Now, we dive into the analytical part of the derived model here.

5 Analysis of Model (5):

5.1 Wellposedness:

To describe wellposedness of the model (5), we have the right-hand side expressions of the equations as f_1, f_2, f_3 and f_4. Similar to the previous system (2)'s wellpossedness, since all the expressions in f_1, f_2, f_3 and f_4 are polynomials so the system in (5) is autonomous and also they are continuously differentiable everywhere. Hence, we have uniqueness and existence of the solutions of the system in (5) on the $\mathbb{R}^4$ interval. Also, the model variables (P, V, P_v, I) have a similar behaviour, where the vector field has the inward trajectories for the positive initial conditions and positive parameter values. Hence, the solutions of the dynamical system are always non-negative as well.

5.2 Equilibria and Stability Analysis of Model (5):

Now we want to focus on calculating the equilibrium solutions of the aggregated model here and analyzing their stability to investigate the model's behaviour. Our main goal here is to understand the impact of infectious pathogens and to investigate the infectious and non-infectious situations. We first try to analyze the stability of the equilibria using the Jacobian, but if it's not possible, we use numerical analysis.

The **Jacobian of the model** (5) for analyzing the stability has the following form.

$$J_A = \begin{bmatrix} -\lambda V - \rho_1 & -\lambda P & 0 & \delta_2 \pi \\ -\lambda V + \beta_2 + \beta_1 K_c & -\lambda P + \gamma(K_c - I) - \rho_2 & 0 & -\gamma V \\ \lambda V & \lambda P & -\sigma_1(K_c - I) - \rho_M & \sigma_1 P_v \\ 0 & 0 & \sigma_1(K_c - I) & -\sigma_1 P_v - \delta_2 \end{bmatrix} \tag{6}$$

5.2.1 Infection Free Equilibrium:

We have an infection-free equilibrium of the model (5), as $E_1 = (P, V, P_v, I) = (0, 0, 0, 0)$ and it is called infection-free, since all the variables become zero in the long run.

Also, we have f_1, f_2, f_3 and f_4 expressions from (5) where all of them are functions of the dependent variables (P, V, P_v, I) and they become zero when all the variables are zero.

Now, to check the stability of the equilibrium here, we use the Jacobian stated at (6), we get:

$$J_A(E_1) = \begin{bmatrix} -\rho_1 & 0 & 0 & \delta_2 \pi \\ \beta_2 + \beta_1 K_c & \gamma K_c - \rho_2 & 0 & 0 \\ 0 & 0 & -\sigma_1 K_c - \rho_M & 0 \\ 0 & 0 & \sigma_1 K_c & -\delta_2 \end{bmatrix} \tag{7}$$

Then from the characteristic polynomial of the Jacobian (7),

$$P_{E_1}(\Lambda) = (\gamma K_c - \rho_2 - \Lambda)(-\rho_1 - \Lambda)(-\sigma_1 K_c - \rho_M - \Lambda)(-\delta_2 - \Lambda) = 0$$

Since, the eigenvalues $-\rho_1, -\sigma_1 K_c - \rho_M, -\delta_2$ are always negative, the infection free equilibrium E_1 is locally asymptotically stable if

$$\gamma K_c - \rho_2 < 0.$$

Thus, E_1 is locally asymptotically stable if $K_c < \frac{\rho_2}{\gamma}$.

5.2.2 Infection Equilibrium:

For the model (5), we first want to find implicit expressions of the infection equilibrium, say $E_2 = (P^*, V^*, P_v^*, I^*)$ in terms of I^*, and also dive into the existence conditions.

We first assume that $P^* \neq 0$, $V^* \neq 0$, $P_v^* \neq 0$ and $I^* \neq 0$ in all the system equations described in (5). Then, from the system being at the equilibrium we have,

$$-\lambda P^* V^* + \delta_2 \pi I^* - \rho_1 P^* = 0 \tag{8}$$
$$-\lambda P^* V^* + \gamma V^* (K_c - I^*) + \beta_2 P^* + \beta_1 P^* K_c - \rho_2 V^* = 0 \tag{9}$$
$$\lambda P^* V^* - \sigma_1 P_v^* (K_c - I^*) - \rho_M P_v^* = 0 \tag{10}$$
$$\sigma_1 P_v^* (K_c - I^*) - \delta_2 I^* = 0 \tag{11}$$

Simplifying equation (11), we have,

$$P_v^* = \frac{\delta_2 I^*}{\sigma_1 (K_c - I^*)} \tag{12}$$

Then also from (10), we get,

$$-\lambda P^* V^* = \frac{-\delta_2 I^* [\sigma_1 (K_c - I^*) + \rho_M]}{\sigma_1 (K_c - I^*)} \tag{13}$$

Now using the simplifications into (8), to get an expression of P^* as a function of I^*,

$$\begin{aligned}
&-\lambda P^* V^* + \delta_2 \pi I^* - \rho_1 P^* = 0 \\
&\Rightarrow \rho_1 P^* = \left[\frac{-\delta_2 [\sigma_1 (K_c - I^*) + \rho_M]}{\sigma_1 (K_c - I^*)} + \delta_2 \pi \right] I^* \\
&\qquad = \frac{I^*}{\sigma_1 (K_c - I^*)} \left[-\delta_2 \sigma_1 (K_c - I^*) - \delta_2 \rho_M + \delta_2 \pi \sigma_1 (K_c - I^*) \right] \\
&\Rightarrow P^* = \frac{-\delta_2 I^*}{\rho_1 \sigma_1 (K_c - I^*)} \left[(1 - \pi) \sigma_1 (K_c - I^*) + \rho_M \right]
\end{aligned} \tag{14}$$

Finally, from (9),

$$\begin{aligned}
&-\lambda P^* V^* + \gamma V^* (K_c - I^*) + (\beta_2 + \beta_1 K_c) P^* - \rho_2 V^* = 0 \\
&\Rightarrow -\lambda_1 P^* V^* + (\beta_2 + \beta_1 K_c) P^* = (\gamma K_c - \gamma I^* - \rho_2) V^* \\
&\Rightarrow -\delta_2 I^* \left(1 + \frac{\rho_M}{\sigma_1 (K_c - I^*)} \right) + (\beta_2 + \beta_1 K_c) \frac{-\delta_2 I^*}{\rho_1 \sigma_1 (K_c - I^*)} \left[(1 - \pi) \sigma_1 (K_c - I^*) + \rho_M \right] = (\gamma K_c - \gamma I^* - \rho_2) V^* \\
&\Rightarrow V^* = \frac{-\delta_2 I^* \left(1 + \frac{\rho_M}{\sigma_1 (K_c - I^*)} \right) + (\beta_2 + \beta_1 K_c) \frac{-\delta_2 I^*}{\rho_1 \sigma_1 (K_c - I^*)} \left[(1 - \pi) \sigma_1 (K_c - I^*) + \rho_M \right]}{(\gamma K_c - \rho_2 - \gamma I^*)}
\end{aligned} \tag{15}$$

So, we have P^*, V^*, P_v^* expressed as a function of I^* here. Before solving for I^* and investigating the exact expression of the infection equilibrium, we observe the existence condition of the infection equilibrium E_2 using the results derived here first.

Existence Conditions:

To explore the existence condition of the equilibrium E_2 here, we use the condition we have from the assumption before that the variables are nonzero, and also, in wellposedness we noticed that the solutions are non-negative. Therefore, we have, $P^* > 0$, $V^* > 0$, $P_v^* > 0$ and $I^* > 0$.

Since we have all the other variables expressed as a function of I^*, we can just directly have an existence condition regarding the I^* variable as $I^* > 0$.

And also since the right side expression of P_v^* in (12) is all positive, so $I^* < K_c$. Therefore, we have an existence condition depending on I^* as,

$$0 < I^* < K_c. \tag{16}$$

We have $P^* > 0$ and from (14), we can write,

$$\frac{-\delta_2 I^*}{\rho_1\sigma_1(K_c - I^*)}\left[(1-\pi)\sigma_1(K_c - I^*) + \rho_M\right] > 0$$

In this expression, we can observe that the $-\delta_2 I^*$ term is negative and $\rho_1\sigma_1(K_c - I^*)$ term is positive. So, the only term we can work with here is $(1-\pi)\sigma_1(K_c - I^*) + \rho_M$, and this term needs to be negative here. Simplifying the expression, we then find another existence condition here:

$$\begin{aligned}
&(1-\pi)\sigma_1(K_c - I^*) + \rho_M < 0 \\
\Rightarrow &-(1-\pi)\sigma_1(K_c - I^*) > \rho_M \\
\Rightarrow &K_c - I^* > \frac{\rho_M}{\sigma_1(\pi - 1)} \\
\Rightarrow &I^* < K_c + \frac{\rho_M}{\sigma_1(1-\pi)}
\end{aligned}$$

We can observe from the equation above that, $K_c + \frac{\rho_M}{\sigma_1(1-\pi)}$ term needs to be larger than I^*. Also, since ρ_M, σ_1 and δ_2 are positive parameters, in the P^* expression, π needs to be greater than 1 for the existence of the infection equilibrium. Therefore, the necessary condition for existence is,

$$\pi > 1 \tag{17}$$

$$I^* < K_c + \frac{\rho_M}{\sigma(1-\pi)} < K_c \tag{18}$$

Finally, from the V^* expression here,

$$\begin{aligned}
V^* &= \frac{-\delta_2 I^*\left(1 + \frac{\rho_M}{\sigma_1(K_c - I^*)}\right) + (\beta_2 + \beta_1 K_c)\frac{-\delta_2 I^*}{\rho_1\sigma_1(K_c - I^*)}\left[(1-\pi)\sigma_1(K_c - I^*) + \rho_M\right]}{(\gamma K_c - \rho_2 - \gamma I^*)} \\
\Rightarrow V^* &= -(\delta_2 I^*)\frac{\rho_1\Big(\sigma_1(K_c - I^*) + \rho_M\Big) + \big(\beta_2 + \beta_1 K_c\big)\left[(1-\pi)\sigma_1(K_c - I^*) + \rho_M\right]}{(\rho_1\sigma_1(K_c - I^*))(\gamma K_c - \rho_2 - \gamma I^*)}
\end{aligned}$$

We now analytically investigate the positivity situation of the V^* variable's expression here, and since $-(\delta_2 I^*)$ is already a negative term, we can have either the numerator is positive when the denominator is negative, or the numerator is negative when the denominator is positive. Therefore, we analyze the following two cases:

For the first case, given that we need $1 < \pi$ and $I^* < K_c + \frac{\rho_M}{\sigma(1-\pi)} < K_c$ for $P^* > 0$, we need,

$$\gamma(K_c - I^*) - \rho_2 < 0 \Rightarrow K_c - \frac{\rho_2}{\gamma} < I^* \tag{19}$$

$$\begin{aligned}
&and \quad \rho_1(\sigma_1(K_c - I^*) + \rho_M) + (\beta_2 + \beta_1 K_c)\left[(1-\pi)\sigma_1(K_c - I^*) + \rho_M\right] > 0 \\
&\Rightarrow \frac{\rho_1}{(\beta_2 + \beta_1 K_c)} > \frac{-\left[(1-\pi)\sigma_1(K_c - I^*) + \rho_M\right]}{(\sigma_1(K_c - I^*) + \rho_M)} > 0 \\
&\Rightarrow \rho_1\sigma_1 K_c - \rho_1\sigma_1 I^* + \rho_1\rho_M > -(\beta_2 + \beta_1 K_c)(1-\pi)\sigma_1 K_c + (\beta_2 + \beta_1 K_c)(1-\pi)\sigma_1 I^* - (\beta_2 + \beta_1 K_c)\rho_M \\
&\Rightarrow (\beta_2 + \beta_1 K_c)(1-\pi)\sigma_1 I^* + \rho_1 I^* < \rho_1\sigma_1 K_c + \rho_1\rho_M + (\beta_2 + \beta_1 K_c)(1-\pi)\sigma_1 K_c + (\beta_2 + \beta_1 K_c)\rho_M \\
&\Rightarrow I^* < \frac{\rho_1(\sigma_1 K_c + \rho_M) + (\beta_2 + \beta_1 K_c)\left[(1-\pi)\sigma_1 K_c + \rho_M\right]}{\sigma_1\left[(\beta_2 + \beta_1 K_c)(1-\pi) + \rho_1\right]}
\end{aligned} \tag{20}$$

For the second case,

$$\gamma(K_c - I^*) - \rho_2 > 0 \Rightarrow K_c - \frac{\rho_2}{\gamma} > I^* \tag{21}$$

$$\begin{aligned} and \quad & \rho_1(\sigma_1(K_c - I^*) + \rho_M) + (\beta_2 + \beta_1 K_c)\left[(1-\pi)\sigma_1(K_c - I^*) + \rho_M\right] < 0 \\ \Rightarrow & \frac{\rho_1}{(\beta_2 + \beta_1 K_c)} < \frac{-\left[(1-\pi)\sigma_1(K_c - I^*) + \rho_M\right]}{(\sigma_1(K_c - I^*) + \rho_M)} \\ \Rightarrow & I^* > \frac{\rho_1(\sigma_1 K_c + \rho_M) + (\beta_2 + \beta_1 K_c)\left[(1-\pi)\sigma_1 K_c + \rho_M\right]}{\sigma_1\left[(\beta_2 + \beta_1 K_c)(1-\pi) + \rho_1\right]} \end{aligned} \tag{22}$$

Explicit Expression of I^*:

To get the explicit forms of the infection equilibrium E_2, we use the other implicit functions of P^*, V^*, P_v^*, and then construct a polynomial of I^* only. This way, we can reduce the whole system to only one variable and then approach to investigate the infection equilibrium.

In the equation (13), we use (15) expression, we get,

$$\begin{aligned} & P^* = \frac{\delta_2 I^*}{\lambda V^*}\left[1 + \frac{\rho_M}{\sigma_1(K_c - I^*)}\right] \\ \Rightarrow & P^* = \frac{\delta_2 I^*\left[1 + \frac{\rho_M}{\sigma_1(K_c - I^*)}\right]}{\lambda \frac{-\delta_2 I^*\left(1 + \frac{\rho_M}{\sigma_1(K_c - I^*)}\right) + (\beta_2 + \beta_1 K_c)\frac{-\delta_2 I^*}{\rho_1 \sigma_1(K_c - I^*)}\left[(1-\pi)\sigma_1(K_c - I^*) + \rho_M\right]}{(\gamma K_c - \rho_2 - \gamma I^*)}} \end{aligned}$$

Now equation this derived expression of P^* with (14), we can find the polynomial of I^*, of the form:

$$AI^{*3} + BI^{*2} + CI^* + D = 0 \tag{23}$$

where,

$$A = \sigma_1\Big[(1-\pi)\lambda\delta_2\left[1 + \frac{(1-\pi)}{\rho_1}(\beta_2 + \beta_1 K_c)\right] + \rho_1\sigma_1\gamma\Big],$$

$$\begin{aligned} B = & -\lambda\delta_2\Big[(1-\pi)(2K_c\sigma_1 + \rho_M) + \rho_M\sigma_1 + \frac{(1-\pi)}{\rho_1}(\beta_2 + \beta_1 K_c)\{\left[2K_c\sigma_1(1-\pi) + \rho_M\right] + \rho_M\sigma_1\}\Big] \\ & - \rho_1\sigma_1\left[(\gamma K_c - \rho_2)\sigma_1 + \gamma(2\sigma_1 K_c + \rho_M)\right], \end{aligned}$$

$$\begin{aligned} C = & \left[\lambda\delta_2(K_c(1-\pi) + \rho_M)\left[(\sigma_1 K_c + \rho_M) + \frac{1}{\rho_1}(\beta_2 + \beta_1 K_c)(\sigma_1 K_c(1-\pi) + \rho_M)\right]\right] \\ & + \rho_1\sigma_1\left[(\gamma K_c - \rho_2)(2\sigma_1 K_c + \rho_M) + K_c\gamma(\sigma_1 + \rho_M)\right], \end{aligned}$$

$$D = -\rho_1\sigma_1 K_c(\sigma_1 K_c + \rho_M)(\gamma K_c - \rho_2),$$

The detailed calculation is written at the end of the report. Since the expressions are vast here, we try to look into some of the numerical cases and analyze the equilibrium more numerically.

Also, in the case of stability analysis, if we use the expressions of the variables in the Jacobian in (6), we get the following matrix:

$$J_A(E_2) = \begin{bmatrix} \lambda\frac{\delta_2 I^*\left(1+\frac{\rho_M}{\sigma_1(K_c-I^*)}\right)+\frac{\delta_2 I^*}{\rho_1\sigma_1(K_c-I^*)}(\beta_2+\beta_1K_c)\left[(1-\pi)\sigma_1(K_c-I^*)+\rho_M\right]}{(\gamma K_c-\rho_2-\gamma I^*)}-\rho_1 \\ \lambda\frac{\delta_2 I^*\left(1+\frac{\rho_M}{\sigma_1(K_c-I^*)}\right)+\frac{\delta_2 I^*}{\rho_1\sigma_1(K_c-I^*)}(\beta_2+\beta_1K_c)\left[(1-\pi)\sigma_1(K_c-I^*)+\rho_M\right]}{(\gamma K_c-\rho_2-\gamma I^*)}+\beta_2+\beta_1K_c \\ \lambda\frac{\delta_2 I^*\left(1+\frac{\rho_M}{\sigma_1(K_c-I^*)}\right)+\frac{\delta_2 I^*}{\rho_1\sigma_1(K_c-I^*)}(\beta_2+\beta_1K_c)\left[(1-\pi)\sigma_1(K_c-I^*)+\rho_M\right]}{(\gamma K_c-\rho_2-\gamma I^*)} \\ 0 \end{bmatrix}$$

$$\begin{matrix} \frac{\lambda\delta_2 I^*}{\rho_1\sigma_1(K_c-I^*)}\left[(1-\pi)\sigma_1(K_c-I^*)+\rho_M\right] & 0 \\ \frac{\lambda\delta_2 I^*}{\rho_1\sigma_1(K_c-I^*)}\left[(1-\pi)\sigma_1(K_c-I^*)+\rho_M\right]+\gamma(K_c-I^*)-\rho_2 & 0 \\ \frac{\lambda\delta_2 I^*}{\rho_1\sigma_1(K_c-I^*)}\left[(1-\pi)\sigma_1(K_c-I^*)+\rho_M\right] & -\sigma_1(K_c-I^*)-\rho_M \\ 0 & \sigma_1(K_c-I^*) \end{matrix} \tag{24}$$

$$\begin{bmatrix} \delta_2\pi \\ \frac{\gamma\delta_2 I^*\left(1+\frac{\rho_M}{\sigma_1(K_c-I^*)}\right)-\frac{\delta_2 I^*}{\rho_1\sigma_1(K_c-I^*)}(\beta_2+\beta_1K_c)\left[(1-\pi)\sigma_1(K_c-I^*)+\rho_M\right]}{(\gamma K_c-\rho_2-\gamma I^*)} \\ \frac{\sigma_1\delta_2 I^*}{\sigma_1(K_c-I^*)} \\ -\delta_2-\frac{\sigma_1\delta_2 I^*}{\sigma_1(K_c-I^*)} \end{bmatrix}$$

Again, to solve the Jacobian for eigenvalues, the equations and expressions are huge, and analytically, they are not interpretable. Therefore, we are unable to construct any stability conditions of the infection equilibrium using the Jacobian. Hence, we shift our focus to having some specific parameter values to study some numerical cases to understand the infection equilibrium behaviour much more thoroughly. Also, all the existence conditions and stability conditions are summarized here in the table 1:

Model	Equilibrium	Existence Condition	Stability Condition
(2)	$(P,V,P_v,H,I)=(0,0,0,0,0)$	–	$b<\delta_1+\delta_2$
(2)	$(P,V,P_v,H,I)=\left(0,0,0,\frac{b-\delta_1}{k},0\right)$	$b-\delta_1>0$	$\frac{\rho_2}{\gamma}>\frac{(b-\delta_1)}{k}$
(5)	$E_1=(P,V,P_v,I)=(0,0,0,0)$	–	$K_c<\frac{\rho_2}{\gamma}$
(5)	$E_2=(P^*,V^*,P_v^*,I^*)$	i. $0<I^*<K_c$ ii. $\pi>1$ iii. $I^*<K_c+\frac{\rho_M}{\sigma(1-\pi)}<K_c$ iv. $K_c-\frac{\rho_2}{\gamma}<I^*$ and $I^*<\frac{\rho_1(\sigma_1K_c+\rho_M)+(\beta_2+\beta_1K_c)\left[(1-\pi)\sigma_1K_c+\rho_M\right]}{\sigma_1\left[(\beta_2+\beta_1K_c)(1-\pi)+\rho_1\right]}$ v. or, $K_c-\frac{\rho_2}{\gamma}>I^*$ and $I^*>\frac{\rho_1(\sigma_1K_c+\rho_M)+(\beta_2+\beta_1K_c)\left[(1-\pi)\sigma_1K_c+\rho_M\right]}{\sigma_1\left[(\beta_2+\beta_1K_c)(1-\pi)+\rho_1\right]}$	–

Table 1: Existence and stability conditions.

5.3 Numerical Results of Model (5):

Analytically, we already observed that the infection equilibrium E_2 has a third-degree polynomial equation for the variable I^*, and so we can expect up to three infection equilibria at a time, depending on the parameter values and sets. Since our approach in this section is to analyze the equilibria and their stability numerically, we must first fix or assume a set of parameter values. In order to set the parameter values here, we find some literature regarding a similar study done in [19].

Now, for the numerical study, we have the following parameter set here:

Parameters	Description	Values	Default values	Reference
λ	binding rate of pathogen and vimentin	-	2.5	Fixed
b	growth rate of epithelial cells	[0.03,0.07]	0.061	[19]
δ_1	apoptosis rate of epithelial cells	[0,0.01]	0.01	[19]
δ_2	Lysis rate of infected epithelial cells	$[10^2, 10^8]$	10^4	[19]
π	pathogen replication factor	[1,10]	10	[19]
ρ_1	removal rate of pathogens due to innate immune system	[0.2,3]	0.5	[19]
γ	autocrine signal producing vimentin rate	-	-	-
β_1	activation rate of vimentin due to inflammation signal	-	1.5×10^{-6}	Fixed
β_2	secretion rate of vimentin due to the presence of pathogen	-	10^{-6}	Fixed
ρ_2	regular removal rate of vimentin	[0.5, 3]	1.8	[19]
σ_1	internalization rate of P-V complex	$[10^{-15}, 10^{-5}]$	10^{-3}	Fixed
ρ_M	trapping rate of P-V complex by macrophages	[0, 0.1]	0.0024	[19]
k	competition rate between cells	47	47	[19]
K_c	carrying capacity of epithelial cells	$[10^2, 10^5]$	10^3	[19]

Table 2: Parameter descriptions and values

From the parameter value table, we can see that we found all the parameter values from other studies, except for λ, γ, β_1, and β_2. We have fixed the values of all the other parameters except the γ parameter. And so, we have numerical solutions of infection equilibrium by varying the γ value here.

Considering the ranges $[10^{-4}, 10^4]$ for the γ parameter, using the ode solver in R Studio to observe the dynamics of number of pathogen, vimentin, P-V complex and infected cell populations with respect to time as well as the phase portraits of pathogen vs infected cell and vimentin vs infected cell. Some of the simulation result is presented in the figure 6.

In figure 6(a) and 6(b), the parameter γ has a lower value of 0.0005 and 0.0016, and P, V, P_v and I dynamics remain low in population in the long run. Also, the phase portraits of vimentin-infected cells and pathogen-infected cells show that the zero equilibrium here is stable, and slight changes in the system do not cause the disease situation to go out of control. The extracellular vimentin here also remains low in number, and it's sufficient for the immune system to clear the infection on its own.

Whereas, the figure 6(c) and 6(d) show oscillatory behaviour in P, V, P_v and I dynamics and also the phase portraits have limit cycles. The peak values for the infected cells and vimentin population are also low. Hence, the equilibrium for these γ values has limit cycles and is stable, which implies that even if the infection occurs again and again, the comparatively low number of extracellular vimentin can help manage the disease situation to stay under control.

Finally, in the last two simulations here in figure 6(e) and 6(f), we can notice that the P, V, P_v, and I cells are extremely high in number. Especially, the number of extracellular vimentin reaches an extremely high value immediately, and the system becomes unstable for the higher value of γ.

To analyze the infection equilibrium numerically here in this study, we use R Studio and, using the coefficients and the third-degree polynomial we derived in (23), we solve for the equilibria of the system in (5). Here, some of the infection equilibria as well as the infection equilibrium for different values of γ are presented in the table 3. We notice that for a lower value of the γ parameter, that is lower rate of autocrine signal producing vimentin, there is only one positive solution of the third-degree polynomial. It changes for higher values of γ, and the detailed analysis is presented in the asymptotic behaviour where we consider γ to be one of the bifurcation parameters and analyze the

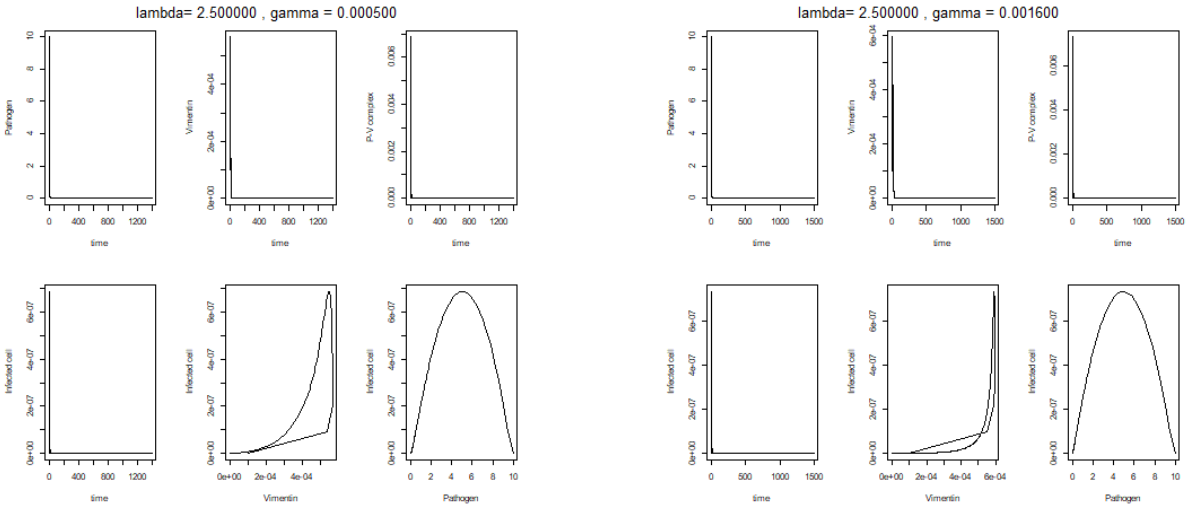

(a)

(b)

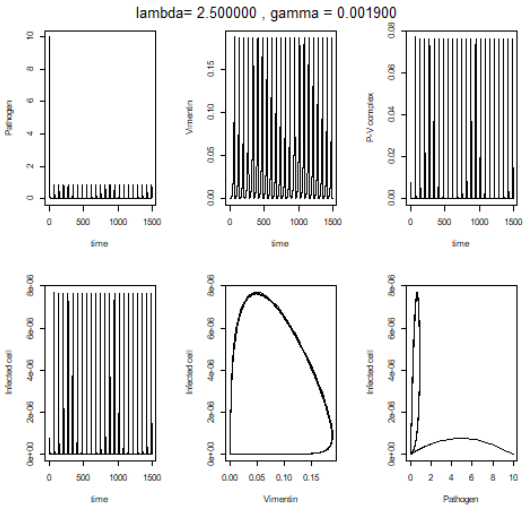

(c)

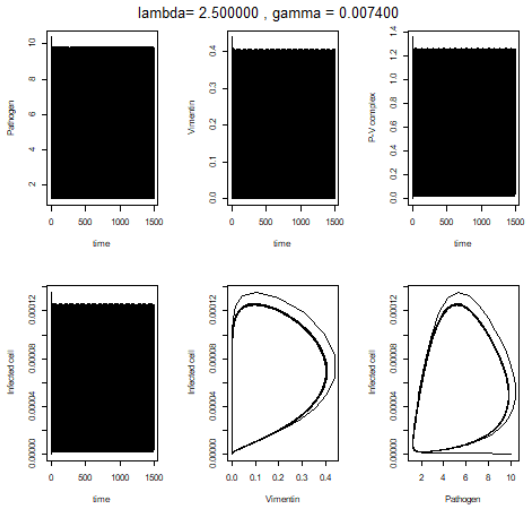

(d)

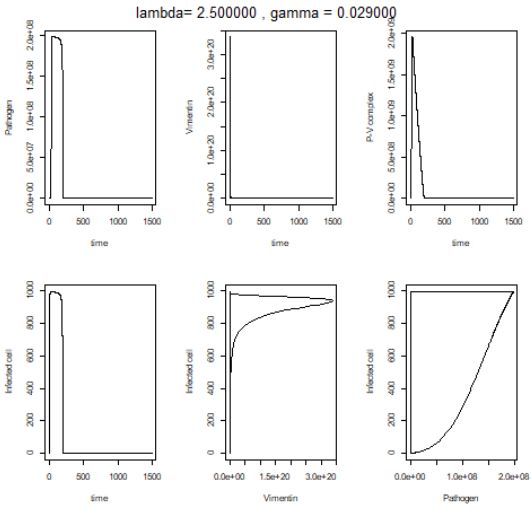

(e)

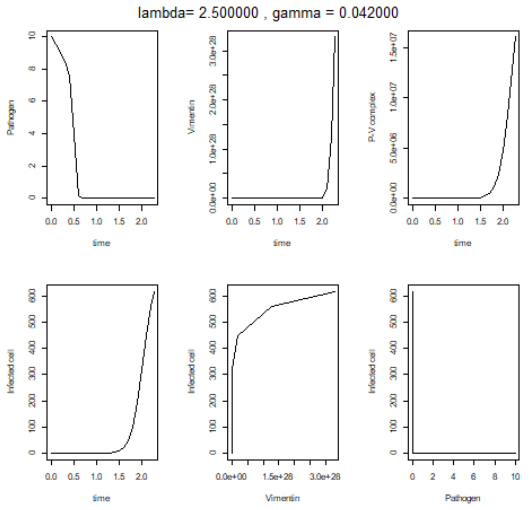

(f)

Figure 6: Numerical solutions are shown in the figure, a) for $\gamma = 0.0005$, b) for $\gamma = 0.0016$, c) for $\gamma = 0.0019$, d) for $\gamma = 0.0074$, e) for $\gamma = 0.029$, and f) for $\gamma = 0.042$. For each value of γ, pathogen (P), vimentin (V), pathogen-vimentin complex (P_v), and infection cell (I) dynamics with respect to time are presented alongside vimentin-infected cell and pathogen-infected cell phase potraits.

equilibria and their nature of stability throughout the different ranges of values.

	γ	IFE	IE	P	V	P_v
1	0.00001	0.00		0.00	0.00	0.00
2	0.00001		4.087933e-09	0.0007356317	2.227556e-05	4.087933e-05
3	0.00002	0.00		0.00	0.00	0.00
4	0.00002		4.065095e-09	0.0007315220	2.227556e-05	4.065095e-05
5	0.00003	0.00		0.00	0.00	0.00
6	0.00003		4.042258e-09	0.0007274123	2.227556e-05	4.042258e-05
7	0.00004	0.00		0.00	0.00	0.00
8	0.00004		4.019420e-09	0.0007233027	2.227556e-05	4.019420e-05
9	0.00005	0.00		0.00	0.00	0.00
10	0.00005		3.996582e-09	0.0007191930	2.227556e-05	3.996582e-05
11	0.00006	0.00		0.00	0.00	0.00
12	0.00006		3.973745e-09	0.0007150833	2.227556e-05	3.973745e-05
13	0.00007	0.00		0.00	0.00	0.00
14	0.00007		3.950907e-09	0.0007109736	2.227556e-05	3.950907e-05
15	0.00008	0.00		0.00	0.00	0.00
16	0.00008		3.928069e-09	0.0007068640	2.227556e-05	3.928069e-05
17	0.00009	0.00		0.00	0.00	0.00
18	0.00009		3.905232e-09	0.0007027543	2.227556e-05	3.905232e-05
19	0.00010	0.00		0.00	0.00	0.00
20	0.00010		3.882394e-09	0.0006986446	2.227556e-05	3.882394e-05

Table 3: Numerical solutions of the model (5).

At this point of numerical analysis, the numerical solutions show different dynamics at different parameter values. We can see that the infection and pathogen drop to zero, then we also see the oscillatory behaviour where the infection peaks and drops down periodically, and then the infection, pathogen, vimentin, and P-V complex explode very promptly. But to interpret the system's biological pattern in the long term more accurately, we turn our focus to analyzing the asymptotic behavior of the infection-free equilibrium (IFE) and the infection equilibrium (IE).

5.4 Asymptotic behaviour Analysis of Model (5):

For the asymptotic behaviour analysis of the model constructed in (5), our goal is to use R programming to find the specific thresholds of steady states or the critical transition points for the equilibria numerically using the earlier derived analytical results. Biologically, we want to interpret and understand how the pathogen infection system defined here is behaving for a long period, and if the extracellular vimentin roles have any significance on infection clearance, or if it chronically stays in the system, or is it not enough to control the infection at all.

We noticed from the analytical results of (5) that we have two different types of equilibrium here. We analyze the asymptotic behaviour for both types of equilibrium here.

5.4.1 Infection Free Equilibrium (IFE) Bifurcation Analysis:

For the given literature values mentioned in Table (2), we find the bifurcation diagram in 7, where we take γ as the bifurcation parameter for the analysis:

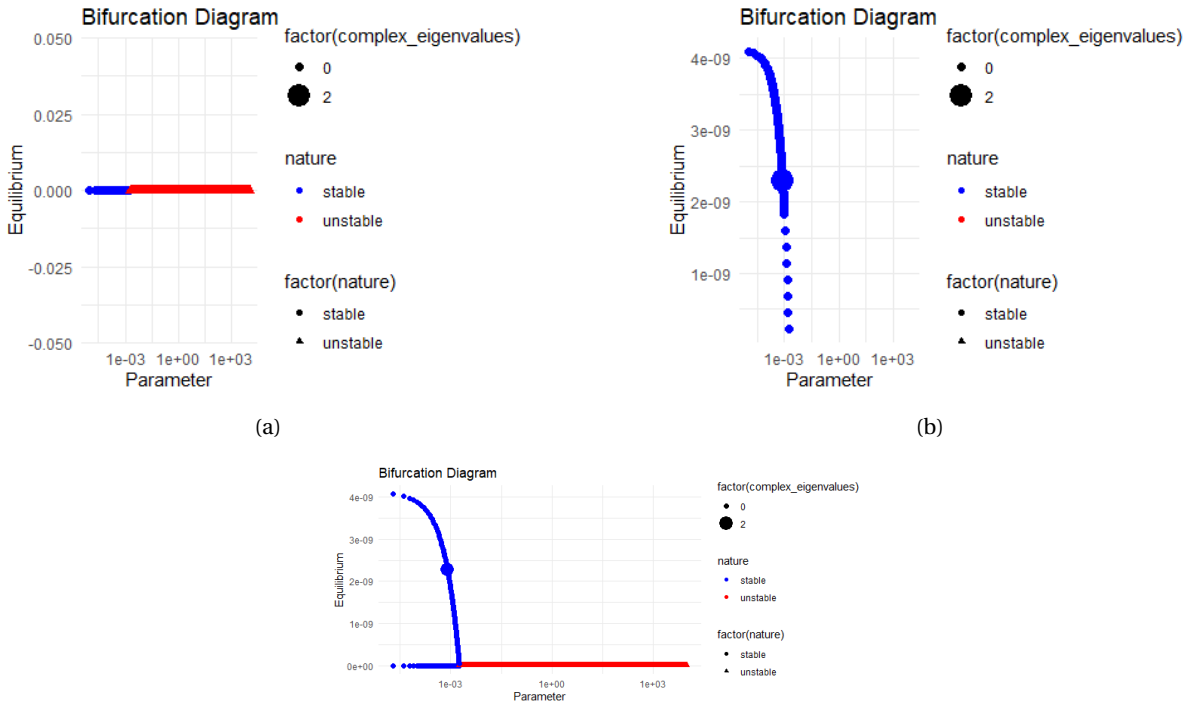

Figure 7: The bifurcation diagram showing stability of the, a) IFE, b) IE, and c) IFE and IE altogether, with varying parameter γ. The figure illustrates the nature of the equilibrium, along with the presence of complex eigenvalues. The blue dots represent the stable equilibria, whereas the red dots represent the unstable equilibria. Also, the bigger shape of the dot indicates that there are complex eigenvalues for that equilibrium.

The bifurcation diagrams in Figure 7 show the nature and number of complex eigenvalues of all the equilibria of model (5) for different values of the γ parameter. The diagram in 7(a) interprets the stability natures of the IFE over the intervals of $[10^{-5}, 10^{4}]$ for γ. For the lower value of the parameter, the IFE is stable, whereas the higher value of γ makes the IFE unstable. For γ in $[10^{-5}, 0.0017]$ the equilibrium is stable and for $\gamma = 0.0019$, the stability switches and becomes unstable. That is, the lower rate of autocrine signal-producing vimentin keeps the system under control and the infection dies out naturally. Also, when the threshold $\gamma = 0.0019$ is reached, the higher rate of autocrine signal producing vimentin more, and the system does not stay infection-free in the long run.

5.4.2 Infection Equilibrium (IE) Bifurcation Analysis:

We have the same set of parameter values, and for the γ parameter, we calculate the infection equilibria and their stability in the bifurcation diagram in Figure 7(b). From the diagram, we can see that the infection equilibria are stable and only exist in the interval $[10^{-5}, 0.0017]$. We can also observe that the infection equilibria are very small and close to zero.

5.4.3 Some Numerical Case Studies for γ:

The asymptotic behaviour analysis here represents the case where we used the available literature data only. And, since we do not have any lab data that can verify the exact behaviour analysis in our specific framework, we consider some of the parameter sets considering possible biological events. This will help us draw some insightful conclusions about the parameters and give us a better understanding of the constructed model's behavior.

Case-1: No Infection Equilibrium

From the existence condition presented earlier, we consider different sets of parameters to present different cases of bifurcation occurring in the system. Again, considering γ to be the bifurcation parameter and changing the parameters $\pi = 0.9$, $\beta_1 = 1.5 * 10^{-4}$ and $\beta_2 = 10^{-4}$. The asymptotic behaviour for these changing parameters is presented in the figure 8.

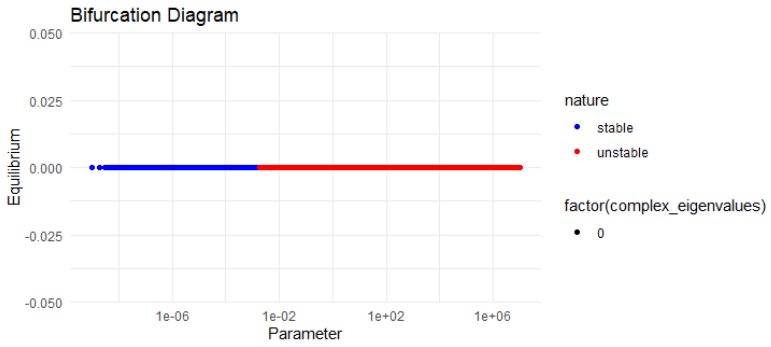

Figure 8: The bifurcation diagram of parameter γ, which shows the stability of the IFE for case-1 (no infection equilibrium). The blue dots are stable IFE, and the red dots are unstable IFE. There are no complex eigenvalues present for the IFE in this case of bifurcation analysis.

The bifurcation diagram for the IFE here shows that the equilibrium is stable for the γ value $<$ 0.0019 and it becomes unstable for the $\gamma \geq 0.0019$ region. Also, it shows that no complex eigenvalues are occurring throughout the whole bifurcation. This can again be interpreted as before. That is when the replication factor of the pathogen is lower than 1, that is $\pi < 1$, the activation and secretion rate of the extracellular vimentin are higher, and the production of the extracellular vimentin due to autocrine signal remain lower than 0.0019 the HPV infection goes away and is cleared out naturally, but if the vimentin production is higher then the infection cannot be cleared out and system becomes unstable.

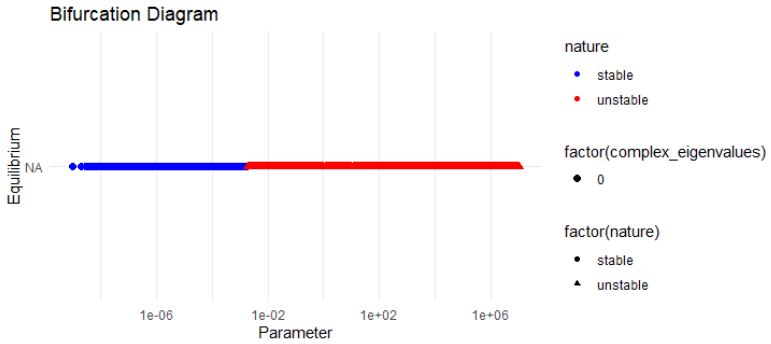

Figure 9: The bifurcation diagram of parameter γ, which shows the stability of the IE for case-1, where the color blue indicates the stable region and red indicates the unstable region. The equilibrium values are all NA, indicating that there are no IE in this diagram.

Similarly, checking the stability of the numerical IE solutions for the specific parameter sets and changing some of the factors, as we stated before, we notice from figure 9, there is no existence of the infection equilibrium in the defined system of the HPV infection.

Phase portraits analysis for case-1

From this case, where we do not have any infection equilibrium, we are only interested in the phase portraits of the infection-free equilibrium. The figure 10 shows different phase potraits for $\gamma = 5 \times 10^{-4}$ and $\gamma = 0.019$, where $\gamma = 5 \times 10^{-4}$ is where the bifurcation diagram in Figure 8 indicates that

the equilibrium is stable and so the other parameter value $\gamma = 0.019$ is the area where the bifurcation diagram shows that the system is unstable.

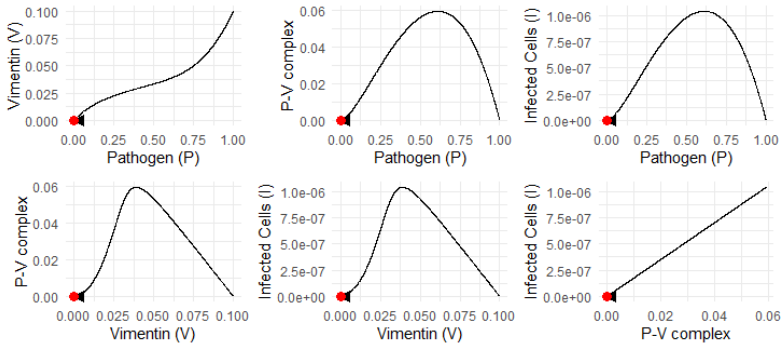

(a)

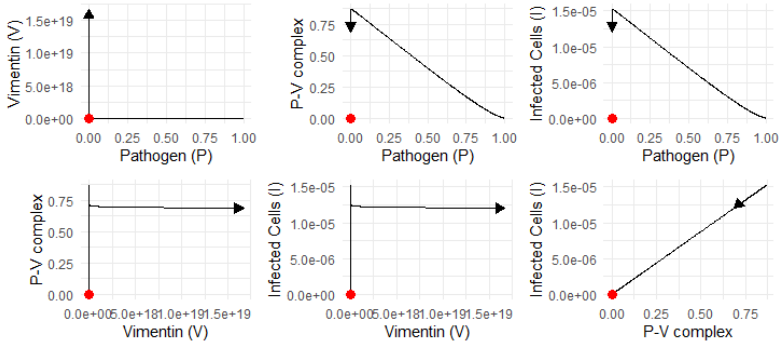

(b)

Figure 10: The phase portraits for all the pairs of state variables are presented here for case 1 (no infection equilibrium) of bifurcation. The phase portraits in figure (a) are for $\gamma = 5 \times 10^{-4}$ and in figure (b) for $\gamma = 0.019$.

In both of the figures in Figure 10, we can observe all the phase portraits for the stable zone of IFE of the system. In this figure, we have phase portraits of P vs V, P vs P_v, P vs I, V vs P_v, V vs I, and P_v vs I, where $\gamma = 5 \times 10^{-4}$ and the red dots are the equilibrium points. It is visually clear to observe the fact that in Figure 10(a), all the phase portraits indicate that the variables go towards the zero red dot, which is the IFE in the long run. The asymptotic behaviour from the bifurcation diagram showed a similar result as well. However, the other phase portraits in Figure 10 show that the pathogen vs vimentin, vimentin vs P-V complex, and the vimentin vs infected cell simulations go away from the equilibrium point, whereas the rest of the phase portraits go towards it. More importantly, if we observe thoroughly, the vimentin population is eventually exploding. Hence, the system is unstable in this parameter range.

Case-2: Existence of Infection Equilibrium

Now, for the second case, we consider another different set of parameters, especially, changing the replication factor of the pathogen, $\pi > 1$. Fixing the exact value at $\pi = 10$, $\beta_1 = 1.5 \times 10^{-4}$, $\beta_2 = 10^{-4}$ and $\rho_2 = 0.5$.Hence, using these values with the rest of the fixed values from the table 2, we analyze the following bifurcation diagrams:

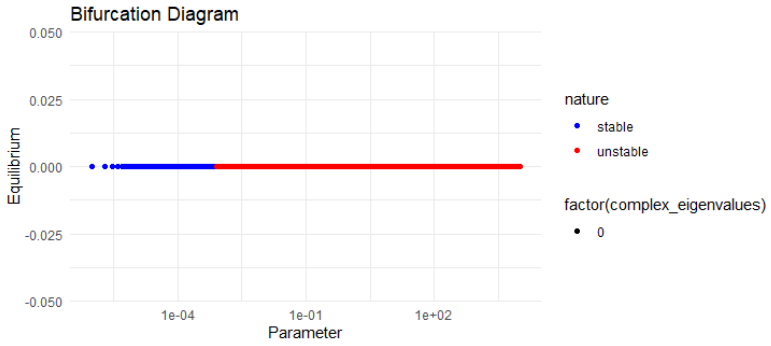

Figure 11: The bifurcation diagram of parameter γ, which shows the stability analysis of the IFE for case-2 (existence of infection equilibrium). The blue color indicates stable equilibrium, and the red color indicates unstable equilibrium.

Here, in the Figure 11, the bifurcation diagram visualize the analysis for the infection-free equilibrium and it shows that, the equilibrium is stable when the system produces extracellular vimentin through the autocrine signal at a lower rate and the exact interval for stability here is $\gamma < 0.000801$. However, when $\gamma \geq 0.000801$, the IFE becomes unstable, which means the HPV infection is cleared out by the vimentin when we have lower production of vimentin, and we have a lower level of infection as well. But when the infection scenario degrades and γ value rises, that means the body is producing more vimentin through the autocrine signal, the infection persists in the long run and cannot be completely eliminated from the system.

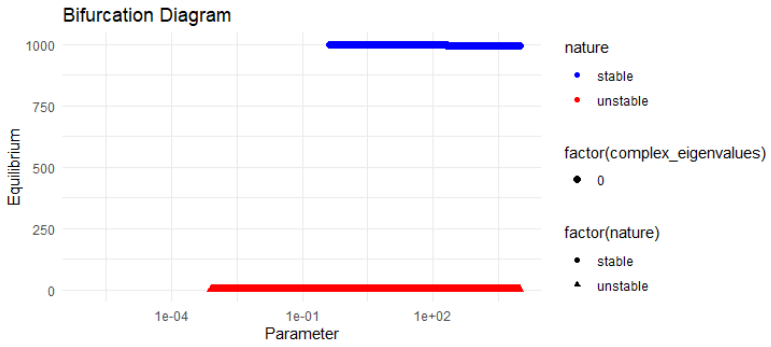

Figure 12: The bifurcation diagram of parameter γ, which shows the stability analysis of the IE for case 2. The colors blue and red are assigned to represent the stable and unstable equilibrium points, respectively. Also, since all the dot shapes are small, there are no complex eigenvalues for the equilibria.

On the other hand, in Figure 12, when we look at the infection equilibrium analysis for higher replication factor and lower regular removal rate of extracellular vimentin, we observe that it starts to appear after a certain value of γ. The infection equilibrium, and in some cases equilibria, start to exist when $\gamma \geq 0.000801$. For the bifurcation parameter interval $[0.000801, 0.437)$, there is only one positive IE in the system, which is very close to zero. This IE is always unstable for $\gamma \geq 0.000801$. In addition to that, when $\gamma \geq 0.437$, there occurs another infection equilibrium which is close to the carrying capacity, and from the diagram we can see that it is stable throughout the whole interval. So, for a comparatively higher production rate of vimentin $\gamma = 0.000801$, the system starts to generate an unstable equilibrium, and even higher production rates lead to the generation of two different-natured non-zero equilibria. Biologically, this can be interpreted as, when there is higher production of extracellular vimentin inside the host body, and the infection peaks, maximum, and eventually, the extracellular vimentin and other immune system components can eliminate the disease situation in the long run. But if the infection equilibrium is low, the HPV infection is unstable, and it does not clear out the pathogen and infection naturally.

Phase portraits analysis for case-2

Now, for this asymptotic behaviour where we do have some infection equilibria, we similarly to before investigate the different phase portraits. The figure 10 shows all the phase potraits for some specific γ va;ue at different stability zones from the bifurcation diagram, $\gamma = 1.0 \times 10^{-6}$, $\gamma = 0.4$ and $\gamma = 5.0 \times 10^{6}$.

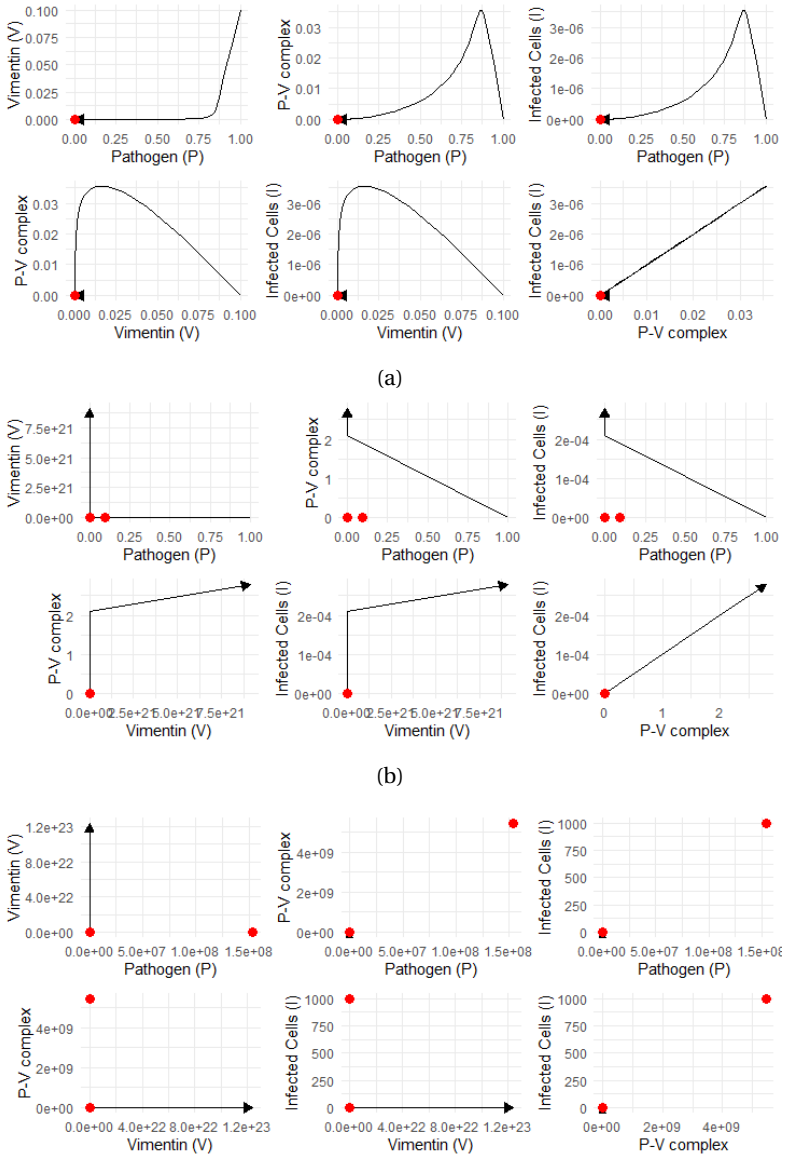

Figure 13: The phase portraits for all the pairs of state variables are presented here for case 2 (stable and unstable infection equilibria) of bifurcation. The phase portraits in figure (a) are for $\gamma = 1.0 \times 10^{-6}$, in figure (b) for $\gamma = 0.4$ and in figure (c) for $\gamma = 5.0 \times 10^{6}$.

Analyzing three different phase portraits from Figure 13, we have all the variable pairs for the phase portrait investigation again. The parameter value $\gamma = 1.0 \times 10^{-6}$ is where the bifurcation diagram shows that the IFE exists and it's stable. Next, $\gamma = 0.4$ is where the infection equilibrium starts to exist, and IFE and IE both are unstable, and finally, we have chosen $\gamma = 5.0 \times 10^{6}$, where IFE is unstable and one of the infection equilibria is stable while the other one is unstable.

Then, simulating the phase portrait over a long time, we can find in Figure 13(a) that everything goes back to the IFE stably as indicated in the bifurcation analysis. Also, Figure 13(b) shows that the trajectories are going away from the red points, which are the equilibria. Lastly, the phase portraits

show empty grids mostly, and due to the very high value generation of the variable values right from the beginning, the ode solver fails to generate solutions properly, indicating the system is extremely stiff and the higher values of the state variables suggesting instability in the infectious situation in real life. Therefore, the asymptotic behaviour fails to understand the patterns accurately due to the stiffness of the parameters of the system. So, next we use a different approach here to analyze the behaviour of the solutions even more.

5.5 Transient behaviour:

After analyzing the long-term pattern of the numerical solutions of the aggregated model defined in (5), we now want to observe the transient behaviours of the steady stable states of the model, specifically the IFE. The importance of this behaviour analysis here is to understand how vastly the system can react even after introducing a small-scale perturbation in the system, hence measuring the reactivity in a short-term period. Also, to understand the character of recovery of the system can be measured, known as resilience. The resilience can help us understand how quickly the system comes back to the equilibrium, or if the system takes a long time before stabilizing itself. Since in the asymptotic behaviour study, we found the variables achieving high values very promptly. The unrealistic and lethal high values of the variables motivate the study of the solutions' perturbation in the short-term period here.

Reactivity and resilience are biological system measures studied in dynamical systems and used to quantify the response to perturbation and the rate of returning to the equilibrium phase of the system [20]. Different models like the food-web model, prey-predator model, as well as discrete ecological models have been studied to find out the transient growth of the environmental systems [21, 22]. The studies show that a temporary amplification of these measures is possible in the prey-predation and food-web system. The upper and lower bound thresholds have also been studied in a biological system where the concepts, restrictions, and methods of calculation of different parameters related to the transient responses have been discussed in detail [23].

Now, in the context of pathogen invasion and infection progression, we apply the calculation of reactivity to describe how the interplay between extracellular vimentin, pathogens, and the immune response reacts to sudden changes and slight perturbations of the system. We then aim to calculate the resilience to observe the biological system's ability to recover after a sudden perturbation in the infection situation in the long run and how quickly the system can go back to and stabilize in the infection-free equilibrium in the presence of extracellular vimentin.

To calculate the transient growth of perturbations of the infection-free equilibrium, we have E_1, we use the Jacobian from (7). Now from [21], we calculate the reactivity using the dominant eigenvalue of the Hermitian matrix and the formula used for the **reactivity** calculation is,

$$\nu_0 = \max_{||x(0)||} \left(\frac{1 d||x||}{||x|| dt} \right) \Big|_{t=0}$$

and the method we use numerically to calculate is, we use the Jacobian matrix at equilibrium J_{E_1} and so we get **reactivity**, $\nu_0(J) = \lambda_1(H(J))$, where λ_1 is the dominant eigenvalue of the hermitian matrix, $H(J) = \frac{1}{2}(J + J^T)$.

Again, to analyze the transient behavior of the infection-free equilibrium of the system, we calculate the resilience of the system and therefore, we use the method of calculating the dominant eigenvalue of the Jacobian matrix, **resilience**, $\nu_\infty = -Re(\lambda_1(J))$, where $Re(\cdot)$ is the real part of the dominant eigenvalue of the linearized system.

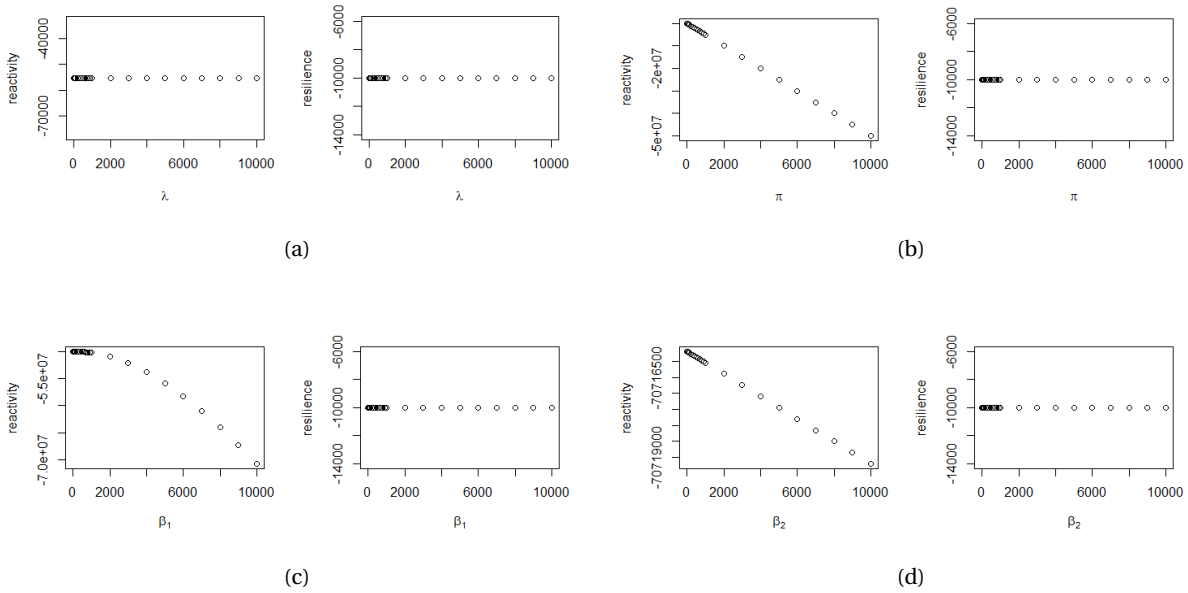

Figure 14: The figure shows transient behaviour analysis in terms of different parameters and their intervals. The reactivity and resilience values are presented for (a) k parameter, (b) π parameter, (c) β_1 parameter, and (d) β_2 parameter here.

Using the expressions defined earlier, we computed the reactivity and resilience for all parameters in the model (5). Figure 14(a) presents the transient behavior of the parameter λ, which represents the binding rate of pathogens to extracellular vimentin. The analysis was conducted over a wide parameter range, $\lambda \in [10^{-4}, 10^{4}]$, where both reactivity and resilience values were plotted against λ. The reactivity remains approximately constant at -5.5×10^4 throughout the interval, indicating that the system is strongly non-reactive to perturbations in λ; small changes in this parameter do not lead to transient amplification of perturbations. Similarly, the resilience remains fixed at -10^4, implying a robust ability of the system to return to the infection-free equilibrium (IFE) after small disturbances, even as λ varies.

A similar trend was observed for the parameters b, δ_1, k, ρ_1, and ρ_M. Each of these showed minimal variation in reactivity and resilience, with consistently large negative values, confirming that the system's dynamics are largely insensitive to short-term changes in these parameters. These findings suggest that the infection-free equilibrium is highly resilient and stable with respect to these biological processes, and the transient dynamics are largely unaffected by moderate variations in their rates.

In contrast, the parameters π, β_1, and β_2 which represent the pathogen replication rate, and the activation and secretion rates of vimentin, respectively exhibit more dynamic transient behavior, as shown in Figures 14(b)–14(d). For π, the reactivity decreases from approximately -9.0×10^6 to -5.0×10^7 as π increases, indicating a monotonic reduction in the system's transient sensitivity. Though reactivity remains negative, its magnitude increases, meaning that perturbations in pathogen replication induce progressively weaker short-term responses. The resilience, however, remains strongly negative and stable, again confirming the system's ability to recover rapidly from perturbations regardless of the value of π. Parameters β_1 and β_2 follow similar trends, reinforcing the interpretation that while the system becomes less transiently responsive as these rates increase, it maintains a high degree of long-term stability. Overall, these findings suggest that π, β_1, and β_2 contribute more noticeably to short-term dynamics compared to λ, b, δ_1, k, ρ_1, and ρ_M, which exert minimal impact on either transient or asymptotic behavior.

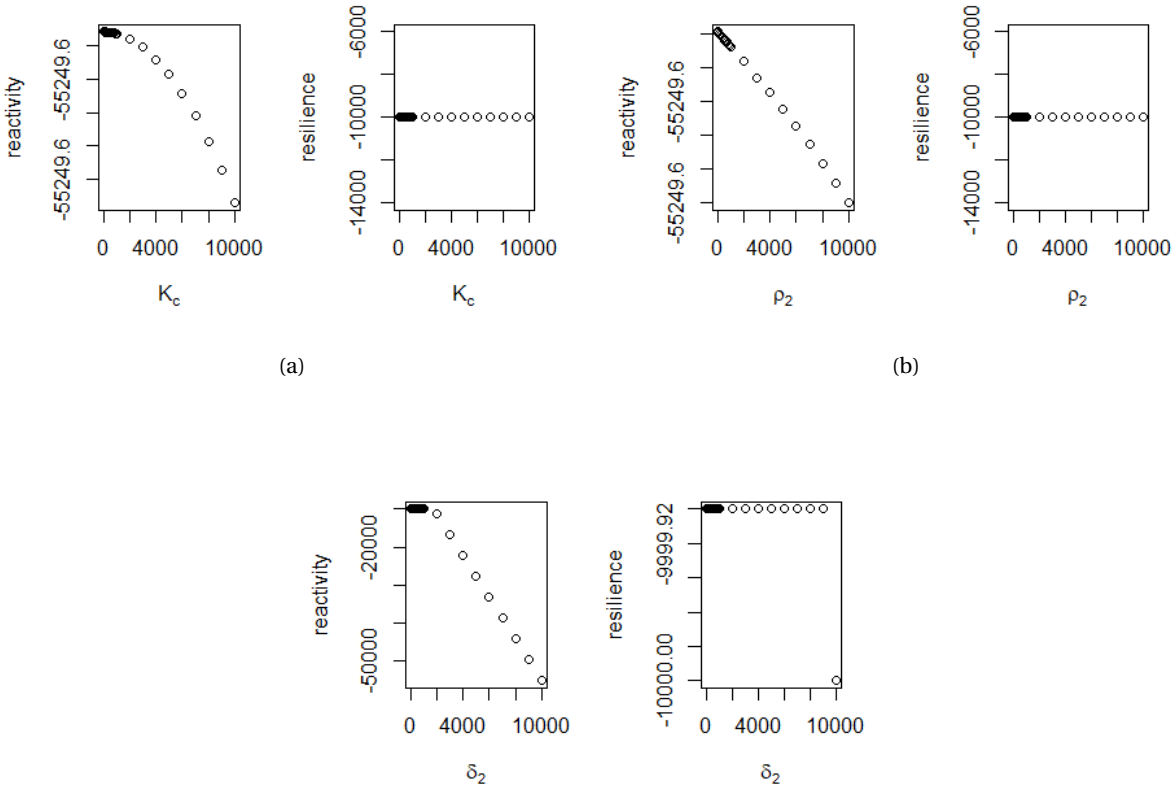

(a)

(b)

(c)

Figure 15: The figure showing transient behaviour analysis for (a) k_c parameter, (b) ρ_2 parameter, and (c) δ_2 parameter here over the interval $[10^{-4}, 10^4]$ on the x-axis.

We further examined the transient dynamics of another group of parameters: K_c, ρ_2, and δ_2, which represent the carrying capacity of epithelial cells, the regular clearance rate of extracellular vimentin, and the lysis rate of infected epithelial cells, respectively. As shown in Figure 15, these parameters exhibit transient behavior that closely mirrors the patterns observed for π, β_1, and β_2 in the earlier analysis.

For the carrying capacity K_c (Figure 15(a)), the reactivity exhibits a modest decline from an initial value of approximately -55249.6 across the interval $[10^{-4}, 10^4]$, while the resilience remains consistently negative throughout. This indicates that changes in the carrying capacity of epithelial cells induce negligible short-term amplification of perturbations and that the system quickly returns to the infection-free equilibrium (IFE), underscoring its high degree of stability.

A similar trend is observed for the clearance rate of extracellular vimentin, ρ_2, and the lysis rate of infected epithelial cells, δ_2, in Figures 15(b) and 15(c), respectively. In both cases, reactivity remains negative and gradually decreases in magnitude as the parameter values increase, signifying that the system becomes progressively less responsive to transient disturbances. Moreover, the resilience profiles are flat and highly negative across the entire interval, reaffirming the system's robust capacity to recover from small perturbations regardless of variations in ρ_2 or δ_2.

These results collectively suggest that K_c, ρ_2, and δ_2 have limited influence on the system's short-term dynamics and do not significantly affect the stability of the infection-free equilibrium. Their roles are likely more supportive or background in nature, contributing to long-term system properties rather than driving transient behavior.

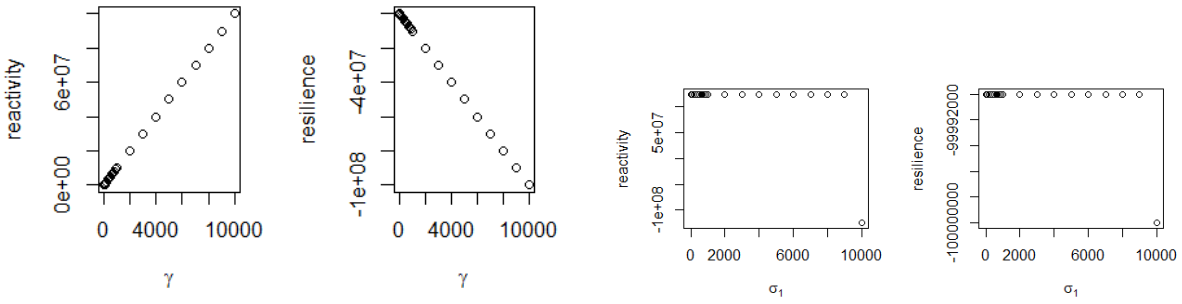

(a) (b)

Figure 16: The figure showing transient behaviour analysis for (a) γ parameter, and (b) σ_1 parameter here over the interval $[10^{-4}, 10^4]$ on the x-axis. The values on the y-axis are the reactivity and resilience values calculated for each parameter of the model, respectively.

Lastly, the transient behavior analysis of parameters γ and σ_1 in Figure 16, which represent the autocrine signaling rate for the extracellular vimentin production and the internalization rate of the pathogens at the cell surface, reveals opposite patterns of effects on the system dynamics in (5). As shown in Figure 16(a), an increase in γ leads to a moderate and steady rise in reactivity, suggesting that stronger autocrine signaling may amplify the system's sensitivity to small perturbations, though not drastically. In contrast, the resilience associated with γ declines linearly, indicating a slower return to equilibrium following disturbances at higher γ values.

On the other hand, for σ_1, shown in Figure 16(b), the reactivity is both high and consistently positive (approximately 10^7), implying that pathogen internalization induces transient instability where small perturbations can initially grow before eventually reducing. However, this reactivity remains nearly constant across the full range of σ_1, suggesting that increasing the internalization rate does not significantly modulate the degree of transient response. Meanwhile, the resilience for σ_1 is strongly negative (approximately -10^9) and also flat, indicating robust long-term stability irrespective of σ_1 levels. Overall, these results imply that while both parameters influence short-term and long-term dynamics, γ provides a more tunable pathway for controlling the system's return to equilibrium, whereas σ_1 primarily contributes to short-term instability without altering the system's overall stability characteristics.

6 Numerical and Asymptotic behaviour Analysis for Parameter π

6.1 Numerical Solutions Varying π Value:

The asymptotic behavior of the mathematical framework can vary significantly based on the parameter under investigation, as different parameters influence the system's sensitivity and long-term dynamics in distinct ways. In this section, we examine the asymptotic behavior of the model defined in equation (5) with respect to the parameter π, which represents the replication factor of the pathogen within the host. Analyzing how the system responds to changes in π provides important insights into the conditions that may lead to persistent infection or pathogen clearance.

The parameters γ and π were chosen for detailed investigation due to their critical biological roles in the infection dynamics. The parameter γ reflects the rate of vimentin production or signaling, which influences the host's cellular response and pathogen interaction. On the other hand, the replication factor π directly governs how rapidly the pathogen multiplies within the host, making it a key driver of disease progression. Exploring the sensitivity of the system to these two parameters allows us to capture both the aggressiveness of the pathogen and the host's defensive mechanisms, providing valuable insights into potential thresholds for infection control and system stability.

Similar to the previous method, we use R Studio to calculate the A, B, C, and D coefficients to generate the equilibrium solutions of the model by solving the polynomial of I in (23). Then, analyze the nature of the solutions by calculating the eigenvalues of the Jacobian matrix of the ODE system from (6). Some of the simulations are presented in the Table 4.

	π	IFE	IE	P	V	Pv	nature
455	6.51	0.00		0.00	0.00	0.00	unstable
456	6.51		1.462749e-04	1.01	0.00	0.15	unstable
457	6.51		915.70	6274324.10	0.13	10862995.65	stable
458	6.52	0.00		0.00	0.00	0.00	unstable
459	6.52		1.337232e-04	0.92	0.00	0.13	unstable
460	6.52		922.18	6333262.33	0.18	11850352.72	stable
461	6.54	0.00		0.00	0.00	0.00	unstable
462	6.54		1.231041e-04	0.85	0.00	0.12	unstable
463	6.54		927.73	6386042.69	0.23	12837706.85	stable
464	6.55	0.00		0.00	0.00	0.00	unstable
465	6.55		1.140035e-04	0.79	0.00	0.11	unstable
466	6.55		932.55	6433895.55	0.30	13825058.04	stable
467	6.57	0.00		0.00	0.00	0.00	unstable
468	6.57		1.061177e-04	0.74	0.00	0.11	unstable
469	6.57		936.76	6477743.97	0.38	14812406.34	stable
470	6.58	0.00		0.00	0.00	0.00	unstable
471	6.58		9.921889e-05	0.69	0.00	0.10	unstable
472	6.58		940.48	6518294.01	0.47	15799751.76	stable
473	6.60	0.00		0.00	0.00	0.00	unstable
474	6.60		9.313300e-05	0.65	0.00	0.09	unstable
475	6.60		943.78	6556094.96	0.59	16787094.33	stable

Table 4: Numerical solutions of the model (5).

Furthermore, we have changed some of the parameter values here to understand one specific case, and multiple different scenarios can also be generated by changing the parameter set. The data used for analyzing the behaviour of π here is provided in Table 5. In addition to that, when we analyze other asymptotic behaviour later regarding π, we use the same set of values.

Parameters	Values
λ	2.5
b	0.061
δ_1	0.01
δ_2	10^3
π	[0,15]
ρ_1	0.8
γ	8×10^{-2}
β_1	1.5×10^{-4}
β_2	10^{-4}
ρ_2	2.2
σ_1	10^{-3}
ρ_M	0.0024
k	47
K_c	10^3

Table 5: Parameter values for numerical analysis of π

6.2 Bifurcation Analysis for Parameter π:

The bifurcation diagrams in Figure 17 illustrate the behavior of the system's equilibria in response to variations in the parameter π, which represents the replication factor of the pathogen. The left panel presents the infection-free equilibria across a range of π values from 0 to 15, while the right panel displays the corresponding infection equilibria.

In the left diagram, the infection-free equilibria are denoted entirely by red markers across all π values, indicating that these equilibria are consistently unstable throughout the parameter range. This suggests that the system cannot maintain a pathogen-free state, regardless of the replication rate.

Conversely, the right diagram reveals more complex dynamics for the infection equilibria. A lower branch of equilibria, appearing from approximately $\pi \approx 6$ onward, is predominantly unstable (marked in red), while a very few number of upper branches of equilibria emerge near the same parameter value $\pi = 6$ and are marked by blue dots, indicating local asymptotic stability. Notably, near the bifurcation point at $\pi \approx 6$, one equilibrium is associated with a pair of complex eigenvalues, suggesting the presence of oscillatory behavior or a transition in stability. Beyond this point, the equilibria are associated with only real eigenvalues, indicating more stable and predictable dynamics. Now, these interesting behaviour exhibited by the diagram motivates us to conduct a deeper analysis at this point.

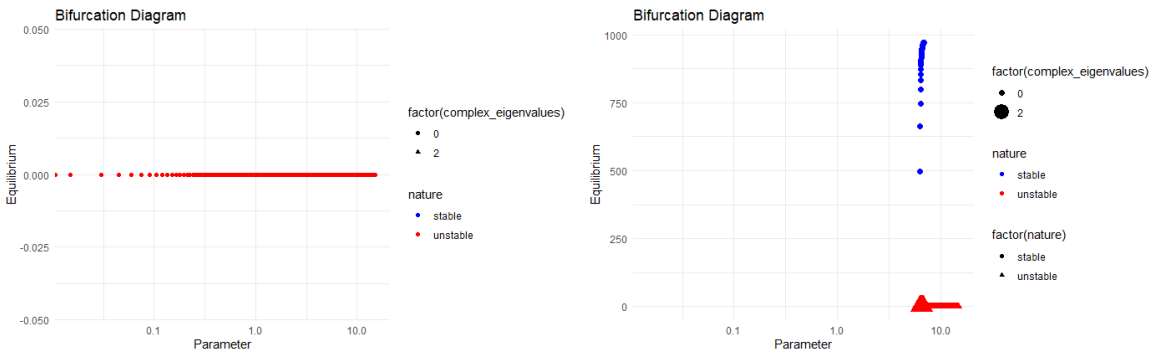

Figure 17: The bifurcation diagram of parameter π, which shows the stability of the infection-free and infection equilibrium.

6.2.1 Phase Portraits Analysis

To better understand the different dynamic regimes suggested by the bifurcation diagram in Figure 17, we present a series of numerical simulations in Figure 18, corresponding to selected values of the pathogen replication factor: $\pi = 0.75$, 4.65, 5.25, 7.2, 11.10, and 13.50. Each subfigure from 18(a) to 18(f) illustrates the time dynamics of four key variables—pathogen (P), extracellular vimentin (V), P-V complex (P_v), and infected cells (I)—under different values of π. Additionally, phase portraits are included to capture the interaction dynamics between infected cells and both vimentin and pathogen levels.

In Figure 18(a), where $\pi = 0.75$, the pathogen population decays rapidly over time, indicating the inability of the pathogen to sustain itself in the host environment. In contrast, the extracellular vimentin level increases drastically and then remains elevated, a potentially destabilizing feature of the system. Both the P-V complex and infected cell populations initially rise before declining, suggesting transient infection and immune engagement. The sharply increasing vimentin level implies a strong biological response despite the low pathogen replication rate, highlighting the potential for vimentin-mediated immune dysregulation in this regime.

In Figure 18(b), with $\pi = 4.65$, both the pathogen and infected cell populations grow rapidly and remain at elevated levels. The infected cells reach their carrying capacity, signaling a fully established infection. Vimentin levels initially spike but then decline to near zero, likely due to consumption of the pathogen binding. Interestingly, the P-V complex also reaches high levels before slightly decreasing, suggesting that the immune response attempts to neutralize the infection but cannot fully eliminate it, leading to a chronic infection state.

Subfigure (c), for $\pi = 5.25$, presents a more stable outcome: all populations rise moderately and then decline to low, steady levels. Notably, vimentin declines to zero, indicating minimal ongoing immune activation. This behavior suggests a possible return to homeostasis or effective pathogen clearance. The phase portraits reveal a nearly complete limit cycle, implying oscillatory dynamics that eventually settle, indicative of a biologically plausible immune regulation process where the system recovers after a transient immune reaction.

In Figure 18(d), corresponding to $\pi = 7.2$, the pathogen, P-V complex, and infected cells all exhibit unbounded or exponential growth, reflecting a breakdown of immune control and progression toward a severe infection. In contrast, the vimentin dynamics are similar to those in subfigure (c), peaking at low levels and diminishing over time. This disparity indicates that the vimentin response is insufficient to counteract the rapidly increasing infection burden, possibly due to exhaustion or evasion mechanisms by the pathogen.

At $\pi = 11.10$, shown in Figure 18(e), the pathogen and infected cells follow sigmoid (S-shaped) growth curves. The pathogen reaches extremely high levels (exceeding 8×10^6), while the infected cells approach the carrying capacity. Vimentin levels remain low throughout, continuing the trend of diminished extracellular immune response at high replication rates. In contrast, the P-V complex exhibits explosive growth, surpassing 3×10^7, possibly indicating excessive immune complex formation and potential cytotoxicity. The absence of limit cycles in the phase portraits suggests the dominance of monotonic progression in disease state without oscillatory feedback.

Finally, in Figure 18(f) with $\pi = 13.50$, the system shows similar behavior to the previous case, but with even more extreme values. All populations increase steeply and remain at high levels, reinforcing the conclusion that high replication rates overwhelm the host immune mechanisms. The lack of oscillations and the dominance of runaway growth in both pathogen and P-V complex populations point toward system instability and possible pathological states such as sepsis or uncontrolled inflammation.

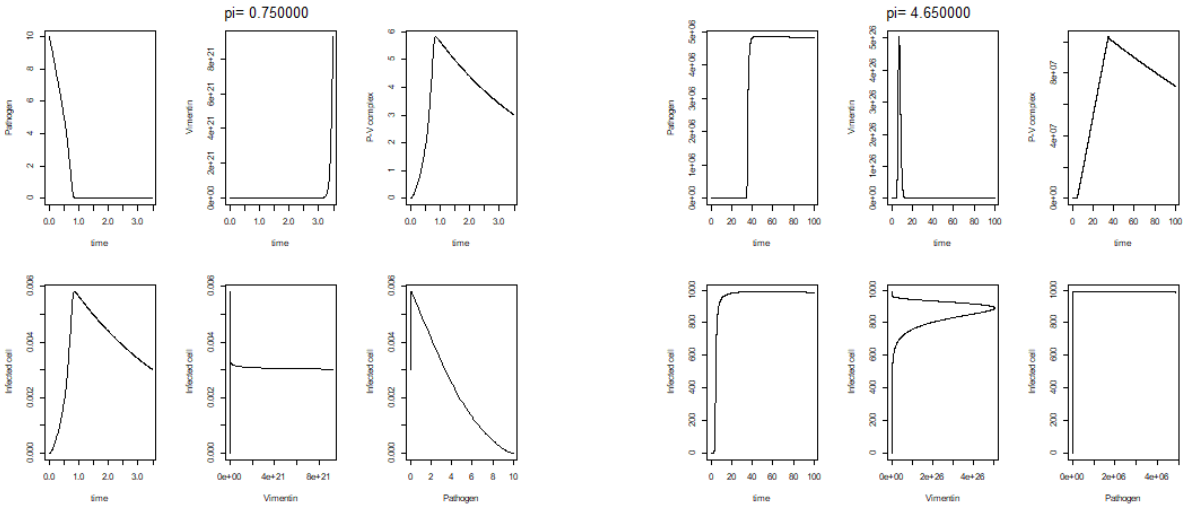

(a)

(b)

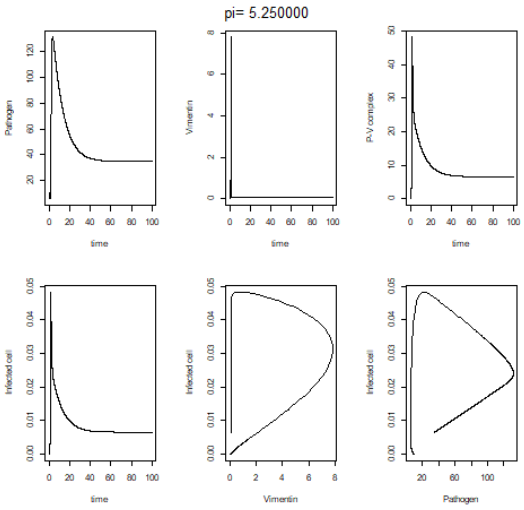

(c)

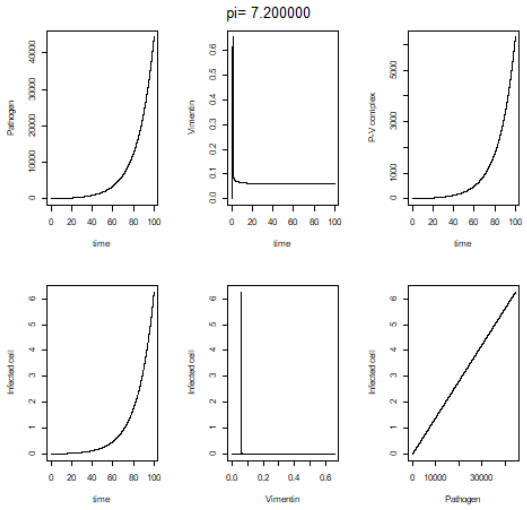

(d)

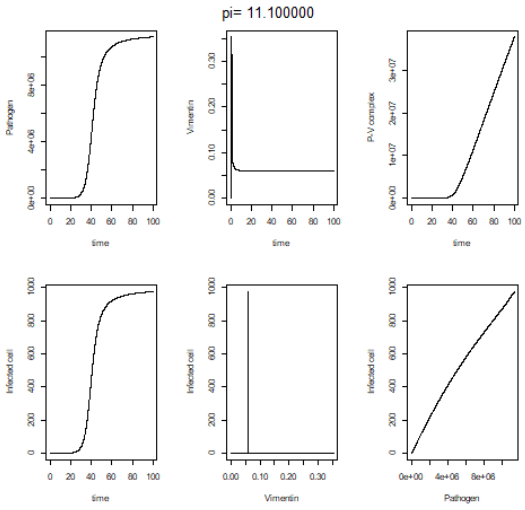

(e)

Figure 18: Numerical solutions where pathogen (P), vimentin (V), pathogen-vimentin complex (P_v), and infection cell (I) dynamics with respect to time are presented alongside vimentin-infected cell and pathogen-infected cell phase potraits are shown in the figure, a) for $\pi = 0.75$, b) for $\pi = 4.65$, c) for $\pi = 5.25$, d) for $\pi = 7.20$, and e) for $\pi = 11.10$.

7 Conclusion and Discussion:

This study conducted here has investigated the role of extracellular vimentin in facilitating pathogen invasion, focusing on its interaction with viral pathogens such as SARS-CoV-2 (COVID-19) and human papillomavirus (HPV). A comprehensive literature review of the existing biological studies was first conducted to establish the biological relevance of extracellular vimentin as a co-receptor or facilitator in pathogen internalization. Besides the internalization process, pathogen and vimentin-related dynamics have been reviewed thoroughly. Specifically, how the extracellular vimentin is secreted and activated at the cell surface while there is the presence of pathogens inside the host, these findings informed the development of a comparatively realistic mathematical model capturing the essential dynamics of this biological interaction.

The model was initially constructed as a five-dimensional nonlinear system of ODEs, representing the interactions among five key populations: pathogens (P), extracellular vimentin (V), pathogen-vimentin complexes (P_v), healthy epithelial cells (H), and infected epithelial cells (I). The 5-variable model in (2) is then analytically studied, where we investigate the equilibria of the model: the zero equilibrium and boundary equilibrium. The stability analysis of the equilibrium showed that the zero equilibrium, $(P, V, P_v, H, I) = (0,0,0,0,0)$, is stable when $b < \delta_1 + \delta_2$, that is when the cell growth rate is smaller than the death rate and the lysis rate of the cells every population we considered goes to the zero equilibrium. The boundary equilibrium, $(P, V, P_v, H, I) = (0,0,0,\frac{b-\delta_1}{k},0)$, is stable when $\frac{\rho_2}{\gamma} > \frac{(b-\delta_1)}{k}$, which means that if the ratio of clearance rate of vimentin and autocrine signal producing viementin is greater than the proliferation of the epithelial cells, then the boundary equilibrium is stable.

Through analytical and biological reasoning, the model was subsequently reduced to a four-dimensional system by aggregating the H and I equations under biologically justified assumptions. This reduction preserved the system's core dynamics while improving analytical traceability. A detailed analysis of the infection-free equilibrium (IFE), E_1, and infection equilibrium, E_2, of the reduced model was conducted using the Jacobian matrix and local stability analysis. The analysis using the Jacobian derived that, E_1 is locally asymptotically stable if $K_c < \frac{\rho_2}{\gamma}$. The stability condition biologically implies that when the ratio of the regular removal rate of vimentin and the production of vimentin through the autocrine signal is greater than the carrying capacity of the epithelial cells, the system comes back to the infection-free equilibrium.

Furthermore, we examined the conditions under which an endemic equilibrium may arise by deriving a third-degree polynomial in I, representing the infected population. This polynomial equation served as a foundation for further numerical and asymptotic analyses.

The asymptotic behavior of the system revealed that certain parameter regimes can lead to rapid, biologically unrealistic increases in pathogen and vimentin concentrations. These results emphasized the need to investigate not only long-term behavior but also the system's transient dynamics, especially around the IFE. For this purpose, reactivity and resilience analyses were employed to quantify how the system initially responds to perturbations and how quickly it returns to equilibrium.

Our results showed that parameters such as the pathogen replication rate (π), the vimentin activation and secretion rates (β_1, β_2), and the autocrine signaling rate of vimentin production (γ) contribute significantly to the system's transient dynamics. These parameters exhibited varying degrees of reactivity, sometimes even positive reactivity, indicating potential biological sensitivity during the early stages of infection. In contrast, parameters such as the carrying capacity of epithelial cells (K_c), the lysis rate of infected cells (δ_2), and the vimentin clearance rate (ρ_2) showed consistently negative and flat reactivity and resilience curves, suggesting strong damping behavior and low sensitivity in the short term.

Lastly, inspired by the transient behavior observed in earlier simulations, we extended our investigation to the pathogen replication factor, denoted by π. While a significant portion of our prior analyses focused on the autocrine signal production rate γ, the role of π warranted a deeper examination due to its biological significance in determining the rate at which the pathogen replicates within

the host. Our bifurcation and numerical analyses reveal that, across the entire estimated range of π, the infection-free equilibrium (IFE) remains persistently unstable. This suggests that even small perturbations near the IFE may lead to unbounded growth in infection, highlighting an intrinsic vulnerability in the system. In contrast, the infection equilibrium (IE) exhibits regions of local asymptotic stability, particularly for a very few values of π, although higher replication rates often result in instability. The corresponding phase portraits show similar findings, showcasing a mix of stable steady states and limit cycle behaviors for a smaller range, depending on the replication rate. These results emphasize the importance of controlling the replication dynamics of the pathogen as a potential strategy for stabilizing the infection outcomes as well.

8 Limitations:

While the current modeling framework offers valuable and important insights into the role of extracellular vimentin in pathogen internalization, it is necessary to recognize several significant limitations that impact its overall scope and applicability. First, the model reduction from a five-dimensional to a four-dimensional system was based on simplifying assumptions concerning the dynamics of healthy and infected epithelial cells. Although these assumptions are biologically motivated and help make the model more tractable, they may overlook complex cellular interactions and processes, including the intricate roles of immune responses, spatial heterogeneity, and cell-to-cell variability, all of which can substantially affect infection progression and the model's predictive accuracy. Second, due to the scarcity of experimentally validated data specific to this context, the parameter analysis relied heavily on hypothetical values and approximations. While sensitivity and bifurcation analyses have been instrumental in identifying influential parameters and understanding the qualitative behavior of the system, the quantitative predictions derived from such analyses may lack precision and real-world relevance, limiting their direct applicability. Third, the model has not yet undergone empirical validation through comparison with in vitro or in vivo experimental data, which restricts the robustness of the biological interpretations and limits confidence in the model's predictive capabilities. Fourth, the biological assumptions for immune response, a critical component in pathogen clearance, inflammation regulation, and tissue repair may have been simplified to construct a simple framework and depending on a more general pathogen related behaviour, and so the model cannot fully capture the long-term host-pathogen dynamics, potentially missing key feedback mechanisms and immune-mediated effects that influence infection outcomes. Lastly, the analysis of transient behavior, which focuses on system properties like resilience and reactivity through local linearization around equilibrium points as well as the numerical and asymptotical calculations for such a stiff system, may not fully show the outcome of the system's response more accurately and may also fail to show results for larger perturbations or nonlinear phenomena. These nonlinear dynamics often play crucial roles in biological systems and can lead to complex behaviors that the current model does not account for, thereby limiting its capacity to predict and explain certain biological responses under varying conditions. Taken together, these limitations highlight important areas for future model refinement and experimental collaboration to enhance the biological fidelity and practical utility of the framework.

References

[1] N. Schwarz and R. E. Leube, "Plasticity of cytoplasmic intermediate filament architecture determines cellular functions," Current Opinion in Cell Biology, vol. 85, p. 102270, 2023.

[2] D. Paulin, A. Lilienbaum, S. Kardjian, O. Agbulut, and Z. Li, "Vimentin: Regulation and pathogenesis," Biochimie, vol. 197, pp. 96–112, 2022.

[3] Ł. Suprewicz, M. Swoger, S. Gupta, E. Piktel, F. J. Byfield, D. V. Iwamoto, D. Germann, J. Reszeć, N. Marcińczyk, R. J. Carroll et al., "Extracellular vimentin as a target against sars-cov-2 host cell invasion," Small, vol. 18, no. 6, p. 2105640, 2022.

[4] A. E. Patteson, A. Vahabikashi, R. D. Goldman, and P. A. Janmey, "Mechanical and non-mechanical functions of filamentous and non-filamentous vimentin," Bioessays, vol. 42, no. 11, p. 2000078, 2020.

[5] J. Arrindell and B. Desnues, "Vimentin: from a cytoskeletal protein to a critical modulator of immune response and a target for infection," Frontiers in immunology, vol. 14, p. 1224352, 2023.

[6] S. Parvanian, L. S. Coelho-Rato, J. E. Eriksson, and A. E. Patteson, "The molecular biophysics of extracellular vimentin and its role in pathogen–host interactions," Current Opinion in Cell Biology, vol. 85, p. 102233, 2023.

[7] Y. T.-C. Yu, S.-C. Chien, I.-Y. Chen, C.-T. Lai, Y.-G. Tsay, S. C. Chang, and M.-F. Chang, "Surface vimentin is critical for the cell entry of sars-cov," Journal of biomedical science, vol. 23, pp. 1–10, 2016.

[8] S. Carse, D. Lang, A. A. Katz, and G. Schäfer, "Exogenous vimentin supplementation transiently affects early steps during hpv16 pseudovirus infection," Viruses, vol. 13, no. 12, p. 2471, 2021.

[9] D. G. Thalla and F. Lautenschläger, "Extracellular vimentin: Battle between the devil and the angel," Current Opinion in Cell Biology, vol. 85, p. 102265, 2023.

[10] P. Deptuła, K. Fiedoruk, M. Wasilewska, Ł. Suprewicz, M. Ciesluk, P. Zeliszewska, M. Ocwieja, Z. Adamczyk, K. Pogoda, and R. Bucki, "Physicochemical nature of sars-cov-2 spike protein binding to human vimentin," ACS applied materials & interfaces, vol. 15, no. 28, pp. 34 172–34 180, 2023.

[11] Z. Yuan, P. A. Janmey, and C. A. McCulloch, "Structure and function of vimentin in the generation and secretion of extracellular vimentin in response to inflammation," Cell Communication and Signaling, vol. 23, no. 1, pp. 1–14, 2025.

[12] C. Miao, S. Zhao, S. Etienne-Manneville, and Y. Jiu, "The diverse actions of cytoskeletal vimentin in bacterial infection and host defense," Journal of Cell Science, vol. 136, no. 1, p. jcs260509, 2023.

[13] Ł. Suprewicz, M. Zakrzewska, S. Okła, K. Głuszek, A. Sadzyńska, P. Deptuła, K. Fiedoruk, and R. Bucki, "Extracellular vimentin as a modulator of the immune response and an important player during infectious diseases," Immunology and Cell Biology, vol. 102, no. 3, pp. 167–178, 2024.

[14] A. Mónico, S. Zorrilla, G. Rivas, and D. Pérez-Sala, "Zinc differentially modulates the assembly of soluble and polymerized vimentin," International journal of molecular sciences, vol. 21, no. 7, p. 2426, 2020.

[15] I. Ramos, K. Stamatakis, C. L. Oeste, and D. Pérez-Sala, "Vimentin as a multifaceted player and potential therapeutic target in viral infections," International journal of molecular sciences, vol. 21, no. 13, p. 4675, 2020.

[16] Z. Li, J. Wu, J. Zhou, B. Yuan, J. Chen, W. Wu, L. Mo, Z. Qu, F. Zhou, Y. Dong et al., "A vimentin-targeting oral compound with host-directed antiviral and anti-inflammatory actions addresses multiple features of covid-19 and related diseases," MBio, vol. 12, no. 5, pp. 10–1128, 2021.

[17] J. R. van Beijnum, E. J. Huijbers, K. van Loon, A. Blanas, P. Akbari, A. Roos, T. J. Wong, S. S. Denisov, T. M. Hackeng, C. R. Jimenez et al., "Extracellular vimentin mimics vegf and is a target for anti-angiogenic immunotherapy," Nature communications, vol. 13, no. 1, p. 2842, 2022.

[18] Ł. Suprewicz, K. Fiedoruk, K. Skłodowski, E. Hutt, M. Zakrzewska, A. Walewska, P. Deptuła, A. Lesiak, S. Okła, P. A. Galie et al., "Extracellular vimentin is a damage-associated molecular pattern protein serving as an agonist of tlr4 in human neutrophils," Cell Communication and Signaling, vol. 23, no. 1, p. 64, 2025.

[19] C. L. Murall, R. Jackson, I. Zehbe, N. Boulle, M. Segondy, and S. Alizon, "Epithelial stratification shapes infection dynamics," PLoS computational biology, vol. 15, no. 1, p. e1006646, 2019.

[20] M. G. Neubert and H. Caswell, "Alternatives to resilience for measuring the responses of ecological systems to perturbations," Ecology, vol. 78, no. 3, pp. 653–665, 1997.

[21] M. G. Neubert, T. Klanjscek, and H. Caswell, "Reactivity and transient dynamics of predator–prey and food web models," Ecological Modelling, vol. 179, no. 1, pp. 29–38, 2004.

[22] H. Caswell and M. G. Neubert, "Reactivity and transient dynamics of discrete-time ecological systems," Journal of Difference Equations and Applications, vol. 11, no. 4-5, pp. 295–310, 2005.

[23] R. E. Snyder, "What makes ecological systems reactive?" Theoretical population biology, vol. 77, no. 4, pp. 243–249, 2010.

Appendix

Calculation of Infection equilibrium of model (5)

To find the infection equilibrium, we start by assuming $P^* \neq 0$, $V^* \neq 0$, $P_v^* \neq 0$, and $I^* \neq 0$ are the infection equilibrium in the aggregated model described in (5). Then we solve the aggregated model equations at equilibrium. First we take the last equation of (5) as below and we achieve an expression of P_v^* as a function of I^*:

$$\begin{aligned}\frac{dI^*}{dt} = 0 &\Rightarrow \sigma_1 P_v (K_c - I) - \delta_2 I = 0 \\ &\Rightarrow \sigma_1 P_v^* (K_c - I^*) = \delta_2 I^* \\ &\Rightarrow P_v^* = \frac{\delta_2 I^*}{\sigma_1 (K_c - I^*)} \end{aligned} \tag{25}$$

Similarly, next we take the differential equation of $\frac{dP_v}{dt}$ at equilibrium and we get,

$$\begin{aligned}\frac{dP_v^*}{dt} = 0 &\Rightarrow \lambda P^* V^* - \sigma_1 P_v^* (K_c - I^*) - \rho_M P_v^* = 0 \\ &\Rightarrow \lambda P^* V^* = [\sigma_1 (K_c - I^*) + \rho_M] P_v^*\end{aligned}$$

Using the P_v^* expression from equation (25) here we get,

$$\lambda P^* V^* = [\sigma_1 (K_c - I^*) + \rho_M] \frac{\delta_2 I^*}{\sigma_1 (K_c - I^*)} \tag{26}$$

$$\Rightarrow \lambda P^* V^* = \delta_2 I^* \left[1 + \frac{\rho_M}{\sigma_1 (K_c - I^*)} \right] \tag{27}$$

Now, from the first equation of the model (5) and using the expression from (25) and (27), we can find,

$$\begin{aligned}&\frac{dP^*}{dt} = -\lambda P^* V^* + \delta_2 \pi I^* - \rho_1 P^* = 0 \\ &\Rightarrow -\delta_2 I^* \left(1 + \frac{\rho_M}{\sigma_1 (K_c - I^*)} \right) + \delta_2 \pi I^* = \rho_1 P^* \\ &\Rightarrow P^* = \frac{-\delta_2 I^*}{\rho_1 \sigma_1 (K_c - I^*)} \left[(1 - \pi) \sigma_1 (K_c - I^*) + \rho_M \right]\end{aligned} \tag{28}$$

Lastly, taking the $\frac{dV}{dt}$ differential equation at equilibrium,

$$\begin{aligned}&\frac{dV^*}{dt} = -\lambda_1 P^* V^* + \gamma V^* (K_c - I^*) + \beta_2 P^* + \beta_1 P^* K_c - \rho_2 V^* = 0 \\ &\Rightarrow -\lambda_1 P^* V^* + (\beta_2 + \beta_1 K_c) P^* = (\gamma K_c - \gamma I^* - \rho_2) V^* \\ &\Rightarrow -\delta_2 I^* \left(1 + \frac{\rho_M}{\sigma_1 (K_c - I^*)} \right) + (\beta_2 + \beta_1 K_c) \frac{-\delta_2 I^*}{\rho_1 \sigma_1 (K_c - I^*)} \left[(1 - \pi) \sigma_1 (K_c - I^*) + \rho_M \right] = (\gamma K_c - \gamma I^* - \rho_2) V^* \\ &\Rightarrow V^* = \frac{-\delta_2 I^* \left(1 + \frac{\rho_M}{\sigma_1 (K_c - I^*)} \right) + (\beta_2 + \beta_1 K_c) \frac{-\delta_2 I^*}{\rho_1 \sigma_1 (K_c - I^*)} \left[(1 - \pi) \sigma_1 (K_c - I^*) + \rho_M \right]}{(\gamma K_c - \rho_2 - \gamma I^*)}\end{aligned} \tag{29}$$

Now, we have all the equations as a function of I^*. Getting another expression of P^* from the expression in (27), we get,

$$P^* = \frac{\delta_2 I^*}{\lambda V^*}\left[1+\frac{\rho_M}{\sigma_1(K_c-I^*)}\right]$$

$$= \frac{\left[1+\frac{\rho_M}{\sigma_1(K_c-I^*)}\right]}{\lambda\frac{-\left(1+\frac{\rho_M}{\sigma_1(K_c-I^*)}\right)-(\beta_2+\beta_1 K_c)\frac{[(1-\pi)\sigma_1(K_c-I^*)+\rho_M]}{\rho_1\sigma_1(K_c-I^*)}}{\gamma K_c-\rho_2-\gamma I^*}}$$

$$Numerator1 = 1+\frac{\rho_m}{\sigma_1(K_c-I^*)} = \sigma_1(K_c-I^*)+\rho_M$$

$$Denominator1 = \left(\lambda\right)\frac{-\left(\sigma_1(K_c-I^*)+\rho_M\right)-\frac{1}{\rho_1}(\beta_2+\beta_1 K_c)\left[(1-\pi)\rho_1(K_c-I^*)+\rho_m\right]}{(\gamma K_c-\rho_2-\gamma I^*)}$$

$$Another \quad P^* = \frac{-\delta_2 I^*}{\rho_1\sigma_1(K_c-I^*)}\left[(1-\pi)(K_c-I^*)+\rho_m\right]$$

$$Numerator2 = -\delta_2 I^*\left[(1-\pi)(K_c-I^*)+\rho_m\right]$$

$$Denominator2 = \rho_1\sigma_1(K_c-I^*)$$

$$Equating \quad P^*,$$

$$\underbrace{Denominator2 * Numerator1}_{\text{LHS}} = \underbrace{Numerator2 * Denominator1}_{\text{RHS}}$$

$$LHS = \rho_1\sigma_1(K_c-I^*)\left[\sigma_1(K_c-I^*)+\rho_M\right]$$

$$= \rho_1\sigma_1^2(K_c-I^*)^2+\rho_1\rho_m\sigma_1(K_c-I^*)$$

$$= \rho_1\sigma_1^2(K_c^2-2K_cI^*+I^{*^2})+\rho_1\rho_m\sigma_1K_c-\rho_1\rho_m\sigma_1I^*$$

$$\boxed{LHS = \rho_1\sigma_1^2I^{*^2}-(2\rho_1\sigma_1^2K_c+\rho_1\sigma_1\rho_m)I^*+\rho_1\sigma_1^2K_c^2+\rho_1\sigma_1\rho_mK_c}$$

$$RHS = -\delta_2 I^*\left[(1-\pi)(K_c-I^*)+\rho_m\right]\left(\lambda\right)\frac{-\left(\sigma_1(K_c-I^*)+\rho_M\right)-\frac{1}{\rho_1}(\beta_2+\beta_1K_c)\left[(1-\pi)\rho_1(K_c-I^*)+\rho_m\right]}{(\gamma K_c-\rho_2-\gamma I^*)}$$

$$= \frac{\delta_2\lambda I^*}{\gamma K_c-\rho_2-\gamma I^*}\Bigg[\underbrace{(1-\pi)(K_c-I^*)\left(\sigma_1(K_c-I^*)+\rho_m\right)}_{\text{1stTerm}}+\underbrace{\frac{1}{\rho_1}(1-\pi)(K_c-I^*)(\beta_2+\beta_1K_c)\left[(1-\pi)\sigma_1(K_c-I^*)+\rho_m\right]}_{\text{2ndTerm}}+$$

$$\underbrace{\rho_M\sigma_1(K_c-I^*)+\rho_M^2}_{\text{3rdTerm}}+\underbrace{\frac{\rho_M}{\rho_1}(\beta_2+\beta_1K_c)\left[(1-\pi)\sigma_1(K_c-I^*)+\rho_m\right]}_{\text{4thTerm}}\Bigg]$$

$$1st \quad Term = (1-\pi)\sigma_1({K_c}^2 - 2K_cI^* + {I^*}^2) + (1-\pi)\rho_M(K_c - I^*)$$
$$= (1-\pi)\sigma_1{I^*}^2 - \left[2K_c(1-\pi)\sigma_1 + (1-\pi)\rho_M\right]I^* + (1-\pi)\sigma_1{K_c}^2 + (1-\pi)\rho_M K_c$$
$$2nd \quad Term = \frac{\sigma_1}{\rho_1}(1-\pi)^2(\beta_2+\beta_1K_c)(K_c-I^*)^2 + \frac{\rho_M}{\rho_1}(1-\pi)(K_c-I^*)(\beta_2+\beta_1K_c)$$
$$= \frac{\sigma_1}{\rho_1}(1-\pi)^2(\beta_2+\beta_1K_c)({K_c}^2 - 2K_cI^* + {I^*}^2) + \frac{\rho_M}{\rho_1}(1-\pi)(K_c-I^*)(\beta_2+\beta_1K_c)$$
$$= \frac{\sigma_1}{\rho_1}(1-\pi)^2(\beta_2+\beta_1K_c){I^*}^2 - \left[2K_c\frac{\sigma_1}{\rho_1}(1-\pi)^2(\beta_2+\beta_1K_c) + \frac{\rho_M}{\rho_1}(1-\pi)(\beta_2+\beta_1K_c)\right]I^*$$
$$+ \frac{\sigma_1}{\rho_1}(1-\pi)^2(\beta_2+\beta_1K_c){K_c}^2 + \frac{\rho_M}{\rho_1}(1-\pi)(\beta_2+\beta_1K_c)K_c$$
$$3rd \quad Term = \rho_M\sigma_1(K_c-I^*) + {\rho_m}^2 = -\rho_m\sigma_1I^* + \rho_m\sigma_1K_c + {\rho_m}^2$$
$$4th \quad Term = \frac{\rho_M}{\rho_1}(\beta_2+\beta_1K_c)(1-\pi)\sigma_1(K_c-I^*) + \frac{{\rho_M}^2}{\rho_1}(\beta_2+\beta_1K_c)$$
$$= -\frac{\rho_M}{\rho_1}(\beta_2+\beta_1K_c)(1-\pi)\sigma_1I^* + \frac{\rho_M}{\rho_1}(\beta_2+\beta_1K_c)(1-\pi)\sigma_1K_c + \frac{{\rho_M}^2}{\rho_1}(\beta_2+\beta_1K_c)$$

Now, there is a rational term in the RHS expression at the beginning, $\frac{\lambda\delta_2 I^*}{\gamma K_c - \rho_2 - \gamma I^*}$. For considering this term in the calculation, let $constant = \lambda\delta_2 I^*$ and $Denom = \gamma K_c - \rho_2 - \gamma I^*$. Now we multiply all the terms of RHS with $constant$:

RHS 1st term × constant
$$= (1-\pi)\sigma_1\lambda\delta_2{I^*}^3 - \lambda\delta_2(1-\pi)\left[2K_c\sigma_1 + \rho_M\right]{I^*}^2$$
$$+ \lambda\delta_2(1-\pi)K_c\left[\sigma_1K_c + \rho_M\right]I^*$$

RHS 2nd term × constant
$$= \frac{\sigma_1\lambda\delta_2}{\rho_1}(1-\pi)^2(\beta_2+\beta_1K_c){I^*}^3$$
$$- \frac{\lambda\delta_2}{\rho_1}(1-\pi)(\beta_2+\beta_1K_c)\left[2K_c\sigma_1(1-\pi) + \rho_M\right]{I^*}^2$$
$$+ \frac{\lambda\delta_2K_c}{\rho_1}(1-\pi)(\beta_2+\beta_1K_c)\left[\sigma_1(1-\pi)K_c + \rho_M\right]$$

RHS 3rd term × constant
$$= -\lambda\delta_2\rho_M\sigma_1{I^*}^2 + \lambda\delta_2\rho_M(\sigma_1K_c + \rho_M)I^*$$

RHS 4th term × constant
$$= -\frac{\lambda\delta_2\rho_M}{\rho_1}(\beta_2+\beta_1K_c)(1-\pi)\sigma_1{I^*}^2$$
$$\frac{\lambda\delta_2\rho_M}{\rho_1}(\beta_2+\beta_1K_c)\left[(1-\pi)\sigma_1K_c + \rho_M\right]I^*$$

And then, we take the $Denom$ from the right side denominator and multiply the left side by the

expression to simplify and group the same order I^* terms to get the polynomial,

$$\begin{aligned}
LHS \times Denom =& (\gamma K_c - \rho_2)\rho_1\sigma_1^2 {I^*}^2 - (\gamma K_c - \rho_2)(2\rho_1\sigma_1^2 K_c + \rho_1\rho_M\sigma_1) I^* \\
&+ (\rho_1\sigma_1^2 K_c^2 + \rho_1\rho_M\sigma_1 K_c)(\gamma K_c - \rho_2) \\
&- \rho_1\sigma_1^2\gamma {I^*}^3 + (2\rho_1\sigma_1^2 K_c + \rho_1\rho_M\sigma_1)\gamma {I^*}^2 \\
&- (\rho_1\sigma_1^2 K_c^2 + \rho_1\rho_M\sigma_1 K_c)\gamma I^* \\
=& -\rho_1\sigma_1^2\gamma {I^*}^3 + \rho_1\sigma_1\left[(\gamma K_c - \rho_2)\sigma_1 + \gamma(2\sigma_1 K_c + \rho_M)\right] {I^*}^2 \\
&- \rho_1\sigma_1\left[(\gamma K_c - \rho_2)(2\sigma_1 K_c + \rho_M) + K_c\gamma(\sigma_1 + \rho_M)\right] I^* \\
&\rho_1\sigma_1 K_c(\sigma_1 K_c + \rho_M)(\gamma K_c - \rho_2)
\end{aligned}$$

Now, using $RHS - LHS = 0$, this gives us the polynomial equation of I^* in the form:

$$A{I^*}^3 + B{I^*}^2 + CI^* + D = 0$$

where,

$$\begin{aligned}
A =& (1-\pi)\sigma_1\lambda\delta_2 + \frac{\sigma_1\lambda\delta_2}{\rho_1}(1-\pi)^2(\beta_2 + \beta_1 K_c) + \rho_1\sigma_1^2\gamma \\
=& \sigma_1\left[(1-\pi)\lambda\delta_2\left[1 + \frac{(1-\pi)}{\rho_1}(\beta_2 + \beta_1 K_c)\right] + \rho_1\sigma_1\gamma\right]
\end{aligned}$$

$$\begin{aligned}
B =& -\lambda\delta_2(1-\pi)\left[2K_c\sigma_1 + \rho_M\right] \\
&- \frac{\lambda\delta_2}{\rho_1}(1-\pi)(\beta_2 + \beta_1 K_c)\left[2K_c\sigma_1(1-\pi) + \rho_M\right] \\
&- \lambda\delta_2\rho_M\sigma_1 \\
&- \frac{\lambda\delta_2\rho_M\sigma_1}{\rho_1}(\beta_2 + \beta_1 K_c)(1-\pi) \\
&- \rho_1\sigma_1\left[(\gamma K_c - \rho_2)\sigma_1 + \gamma(2\sigma_1 K_c + \rho_M)\right] \\
\Rightarrow B =& -\lambda\delta_2\Big[(1-\pi)(2K_c\sigma_1 + \rho_M) + \rho_M\sigma_1 + \frac{(1-\pi)}{\rho_1}(\beta_2 + \beta_1 K_c)\{\left[2K_c\sigma_1(1-\pi) + \rho_M\right] + \rho_M\sigma_1\}\Big] \\
&- \rho_1\sigma_1\left[(\gamma K_c - \rho_2)\sigma_1 + \gamma(2\sigma_1 K_c + \rho_M)\right]
\end{aligned}$$

$$\begin{aligned}
C =& \lambda\delta_2 K_c(1-\pi)\left[\sigma_1 K_c + \rho_M\right] \\
&+ \frac{\lambda\delta_2 K_c}{\rho_1}(1-\pi)(\beta_2 + \beta_1 K_c)\left[\sigma_1 K_c(1-\pi) + \rho_M\right] \\
&+ \lambda\delta_2\rho_M(\sigma_1 K_c + \rho_M) \\
&+ \frac{\lambda\delta_2\rho_M}{\rho_1}(\beta_2 + \beta_1 K_c)\left[(1-\pi)\sigma_1 K_c + \rho_M\right] \\
&+ \rho_1\sigma_1\left[(\gamma K_c - \rho_2)(2\sigma_1 K_c + \rho_M) + K_c\gamma(\sigma_1 + \rho_M)\right] \\
\Rightarrow C =& \left[\lambda\delta_2(K_c(1-\pi) + \rho_M)\left[(\sigma_1 K_c + \rho_M) + \frac{1}{\rho_1}(\beta_2 + \beta_1 K_c)(\sigma_1 K_c(1-\pi) + \rho_M)\right]\right] \\
&+ \rho_1\sigma_1\left[(\gamma K_c - \rho_2)(2\sigma_1 K_c + \rho_M) + K_c\gamma(\sigma_1 + \rho_M)\right]
\end{aligned}$$

And,

$$D = -\rho_1\sigma_1 K_c(\sigma_1 K_c + \rho_M)(\gamma K_c - \rho_2)$$